Stem Cell Reports
Article

ISSCR

OPEN ACCESS

Enhancing Hematopoiesis from Murine Embryonic Stem Cells through MLL1-Induced Activation of a Rac/Rho/Integrin Signaling Axis

Weiwei Yang,[1,6] G. Devon Trahan,[1] Elizabeth D. Howell,[7] Nancy A. Speck,[7] Kenneth L. Jones,[1] Austin E. Gillen,[3] Kent Riemondy,[3] Jay Hesselberth,[3] David Bryder,[4,5] and Patricia Ernst[1,2,*]

[1]Department of Pediatrics, Section of Hematology/Oncology/BMT University of Colorado, Denver/Anschutz Medical Campus, Aurora, CO 80045, USA
[2]Department of Pharmacology, University of Colorado, Denver/Anschutz Medical Campus, Aurora, CO 80045, USA
[3]RNA Biosciences Initiative, University of Colorado, Denver/Anschutz Medical Campus, Aurora, CO 80045, USA
[4]Division for Molecular Hematology, Lund Stem Cell Center, Lund University, B10 221 84 Lund, Sweden
[5]Sahlgrenska Cancer Center, University of Gothenburg, 405 30 Gothenburg, Sweden
[6]Department of Molecular and Systems Biology, Geisel School of Medicine at Dartmouth, Hanover, NH 03755, USA
[7]Abramson Family Cancer Research Institute, Department of Cell and Developmental Biology, Institute for Regenerative Medicine, Perelman School of Medicine at the University of Pennsylvania, Philadelphia, PA 19104, USA
*Correspondence: patricia.ernst@cuanschutz.edu
https://doi.org/10.1016/j.stemcr.2019.12.009

SUMMARY

The *Mixed Lineage Leukemia* (*MLL1*, *KMT2A*) gene is critical for development and maintenance of hematopoietic stem cells (HSCs), however, whether this protein is limiting for HSC development is unknown due to lack of physiologic model systems. Here, we develop an MLL1-inducible embryonic stem cell (ESC) system and show that induction of wild-type MLL1 during ESC differentiation selectively increases hematopoietic potential from a transitional c-Kit$^+$/Cd41$^+$ population in the embryoid body and also at sites of hematopoiesis in embryos. Single-cell sequencing analysis illustrates inherent heterogeneity of the c-Kit$^+$/Cd41$^+$ population and demonstrates that MLL1 induction shifts its composition toward multilineage hematopoietic identities. Surprisingly, this does not occur through increasing *Hox* or other canonical MLL1 targets but through an enhanced Rac/Rho/integrin signaling state, which increases responsiveness to Vla4 ligands and enhances hematopoietic commitment. Together, our data implicate a Rac/Rho/integrin signaling axis in the endothelial to hematopoietic transition and demonstrate that MLL1 actives this axis.

INTRODUCTION

Studying embryonic stem cell (ESC) differentiation *in vitro* has contributed to understanding early developmental processes while identifying methods to direct differentiation of specific cell types potentially useful to treat a variety of pathophysiologic conditions (Keller, 2005). Despite remarkable progress made over two decades, it is not yet feasible to produce hematopoietic stem and progenitor cells (HSPCs) from ESCs that engraft and persist in recipients (Ditadi et al., 2017; Rowe et al., 2016). In vertebrates, hematopoiesis occurs in successive waves, producing diverse progenitors with specific potentials (Dzierzak and Bigas, 2018; Dzierzak and Speck, 2008). The first wave is initiated in the yolk sac (YS) blood islands and gives rise to a transient population of primitive red blood cells, diploid megakaryocytes, and primitive macrophages (Bertrand et al., 2005; Palis et al., 1999; Tober et al., 2007). A second wave initiating in the YS gives rise to definitive erythroid and myeloid progenitors (EMPs) (Lux et al., 2008; McGrath et al., 2015; Palis et al., 1999). A third wave occurs at embryonic (E) day 10.5 in the major arteries: the dorsal aorta, vitelline artery, and umbilical artery of the aorta-gonad-mesonephros (AGM) region (Dzierzak and Speck, 2008); this is the first site at which transplantable hematopoietic stem cells (HSCs) are produced. These HSCs and the earlier multipotent progenitors are thought to arise from specialized endothelium (hemogenic endothelium [HE]) through an endothelial to hematopoietic transition (EHT) (Bertrand et al., 2010; Boisset et al., 2010; Eilken et al., 2009; Frame et al., 2016; Lancrin et al., 2009). *In vitro* differentiation of ESCs from embryoid bodies (EBs) generally recapitulates YS hematopoiesis, and efforts have been made to direct differentiation to produce transplantable HSCs by manipulating intrinsic or extrinsic signals (Ditadi et al., 2017). Although not all types of progenitor cells can be produced from ESCs *in vitro*, the fact that developmental processes including EHT can be manipulated pharmacologically and genetically makes this system a valuable model to study how hematopoietic commitment occurs and can be influenced (Lancrin et al., 2009).

Mll1 (Kmt2a) loss-of-function murine models implicated this gene as a major regulator of HSPC development and homeostasis including in EBs and embryos (Ernst et al., 2004a; Jude et al., 2007; McMahon et al., 2007; Yang and Ernst, 2017). Our prior findings that MLL1 regulates an HSC-specific target gene repertoire led us to wonder whether increasing MLL1 levels could have an impact on hematopoietic development during the early waves of

hematopoiesis. This question, however, has been difficult to address due to the absence of appropriate model systems.

The human *MLL1/KMT2A* gene is a frequent target of chromosomal translocations that cause acute leukemias (Krivtsov and Armstrong, 2007). Most translocations produce fusions that exhibit ectopic transactivation capacity. However, partial tandem duplications within the MLL1 gene (MLL-PTD) and occasional cases of *MLL1* amplification have been reported in myelodysplastic syndrome and acute myeloid leukemia (AML), often concomitant with upregulation of MLL1 target genes such as *HOXA7*, *HOXA9*, and *MEIS1* (Dorrance et al., 2006; Poppe et al., 2004; Tang et al., 2015). Attempts to determine the impact of these non-fusion events or to test the latent oncogenic potential of wild-type (WT) MLL1 protein have been hampered by the challenges of expressing the large *MLL1* cDNA and the fact that MLL1 overexpression arrests cell growth (Joh et al., 1996; Liu et al., 2007). Thus, having a model that enables increasing MLL1 levels would be of great significance for multiple mechanistic avenues of investigation. In the current study, we developed a system in which WT MLL1 can be induced within physiologically tolerated ranges. This system revealed that increasing MLL1 protein level only by ~2-fold enhanced hematopoietic potential. These data also highlight the role of Rac/Rho/integrin signaling during the EHT.

RESULTS

Generation and Validation of WT hMLL1-Inducible ESCs

To achieve consistent and reversible induction of MLL1 *in vitro* and *in vivo*, we generated a doxycycline-inducible MLL1 human (hMLL1i) transgene by integrating a modified cDNA into the murine *Col1a1* locus (Beard et al., 2006) (Figures S1A and S1B). Human and mouse MLL1 proteins are 93% similar, and human fusion oncoproteins function in murine cells. Maximal induction of hMLL1 occurred at addition of 2 μg/mL doxycycline, which corresponded to an approximately 2-fold increase in total MLL1 protein (Figures 1A, 1B, and S1C–S1E). To determine whether H3K4 methylation levels were altered by this increase, we performed western blots on extracted histones (Figure S1F). Consistent with prior results indicating that MLL1 is not a dominant H3K4 methyltransferase (Denissov et al., 2014; Mishra et al., 2014), we found that H3K4me1/2/3 levels were not altered, despite significant changes in gene expression. Co-immunoprecipitation of Menin and Wdr5 demonstrated that induced MLL1 is functional and associates with known complex components (Figures S1G–S1I). Thus, we have developed a system in which physiologically tolerated induction of WT MLL1 can be achieved.

hMLL1 Induction Does Not Grossly Alter ESC Differentiation

To first determine whether increasing MLL1 protein influenced germ layer specification and differentiation, several regimens of induction were tested (Figure S1J). EBs generated from differentiated ESCs ± hMLL1 induction throughout the time course exhibited similar morphology and cell accumulation during differentiation (Figures 1C and 1D). This was true whether hMLL1 induction was performed throughout differentiation or during brief phases of differentiation (Figure 1D). Genes characteristic of each of the three germ layers were expressed normally in all regimens (Figures 1E–1G). Thus, maximal hMLL1 induction does not grossly alter overall EB differentiation, cell survival, or proliferation.

Induction of hMLL1 Does Not Significantly Alter Mesoderm Differentiation

The production of hematopoietic cells in EBs occurs through developmental steps paralleling hematopoiesis in the YS of the embryo (Rowe et al., 2016). Flk-1 expression encompasses mesodermal cells committed to hematopoietic, endothelial, cardiogenic, and muscle fates (Kattman et al., 2006; Lugus et al., 2009; Shalaby et al., 1997). In our system, Flk-1$^+$ cells peak at day 4 of EB differentiation, and this is not altered by hMLL1 induction (Figure 2A). Flk-1$^+$ cells encompass both Pdgfrα$^+$ and Pdgfrα^{neg}; Flk1$^+$/Pdgfrα$^+$ cells are cardiogenic, whereas Flk-1$^+$/Pdgfrα^{neg} cells contain precursors of endothelial and hematopoietic lineages (Kataoka et al., 2011). Flk-1$^+$/Pdgfrα^{neg} cells give rise to a small population of HE cells that are Cd41^{low}/VE-cadherin$^+$/Tie-2$^+$, which in turn differentiate into Cd41^{hi}/Cd45$^+$ cells that include hematopoietic progenitor cells (Choi et al., 1998; Eilken et al., 2009; Kennedy et al., 2007; Lancrin et al., 2009; Robertson et al., 2000). To test the impact of hMLL1 induction on this developmental progression, we induced hMLL1 during days 2–4 or days 4–7 and determined population frequencies by flow cytometry. hMLL1 induction did not alter Flk-1$^+$/Pdgfrα^{neg} cell generation (Figure 2B). HE cells (c-Kit$^+$/Tie-2$^+$) were produced in EBs with similar kinetics and in similar proportions except for a small reduction at day 7 in hMLL1-induced cultures (Figures 2C, S2A, and S2B). Acquisition of hematopoietic markers (Cd41^{hi}/Cd45$^+$) (Gritz and Hirschi, 2016) proceeded similarly regardless of hMLL1 induction (Figure 2D). These data show that overall specification of hemogenic endothelial precursors, as defined immunophenotypically, occurs independent of MLL1 levels.

Induction of hMLL1 Selectively Affects c-Kit$^+$/Cd41$^+$ Hematopoietic Progenitor Function

To determine whether the emergence of hematopoietic potential was influenced by hMLL1 induction, we determined c-Kit$^+$/Cd41$^+$ cell frequencies, which represent the first population enriched in multilineage hematopoietic

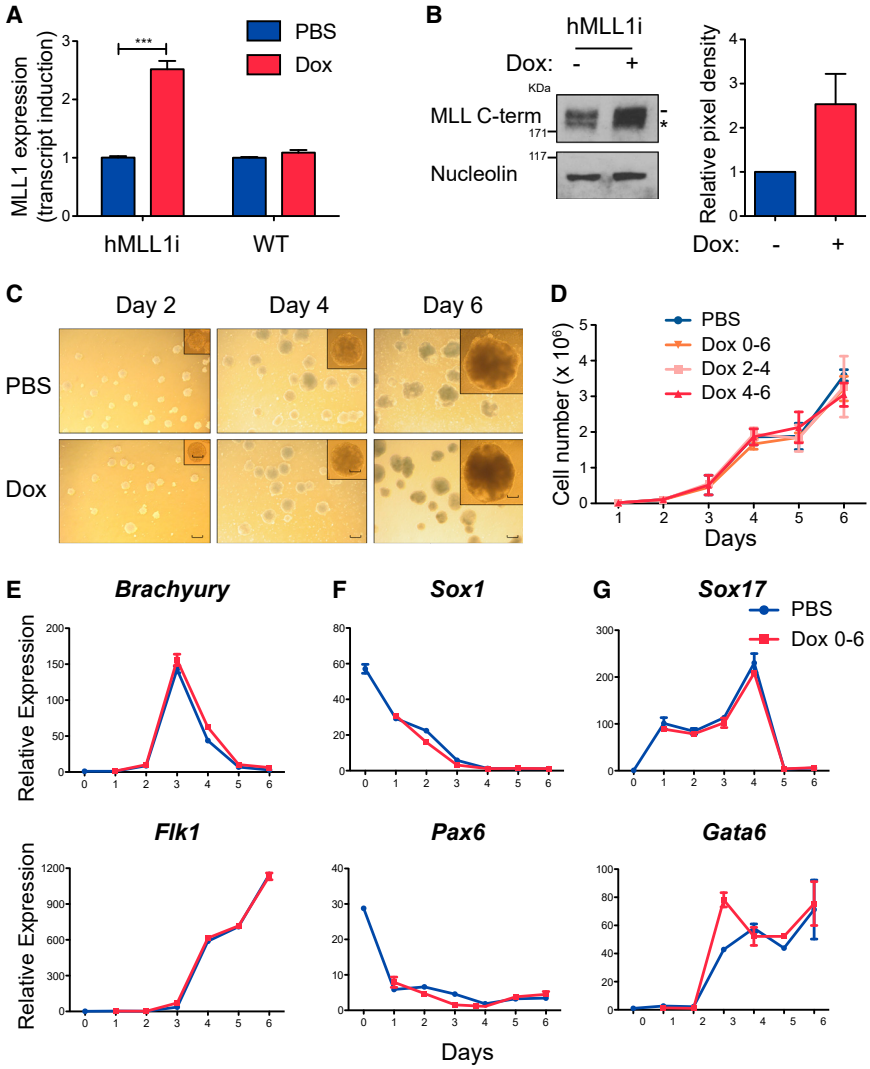

Figure 1. Induction of Physiologic Levels of WT hMLL1 Does Not Perturb Normal EB Differentiation

(A) Quantitative RT-PCR showing total murine + human transcript. WT (KH2) or hMLL1-inducible ESCs were harvested 48 h after doxycycline (Dox) treatment. Phosphate buffered saline (PBS) is the solvent control. Bar graph represents average expression (relative to *Gapdh*) of total *Mll1/MLL1* transcript from three independent experiments ± SEM.

(B) Western blot showing induced MLL1 protein. Nuclear protein was extracted from hMLL1-inducible ESCs ± Dox. Nucleolin represents the loading control. The dash shows the MLL1 C terminal peptide (p180); the asterisk marks the degradation product. Quantification reflects western blots from three independent experiments.

(C) Images showing morphology of EBs from day 2 to day 6 at 40× magnification. Scale bar for inset, 22.6 mm. Scale bar for bigger picture, 48.9 mm.

(D) EB accumulation in different induction schemes. One representative from three independent experiments is shown. Data represent average cell numbers ± SEM, n = quadruplicate cultures. Experiments were performed with hMLL1-inducible ESCs. Dox 0–6 = doxycycline added to differentiation medium from day 0 to day 6; Dox 2-4, doxycycline added to differentiation medium from day 2 to day 4; Dox 4-6 = doxycycline added to differentiation medium from day 4 to day 6.

(E–G) Representative gene expression of (E) mesoderm (*Brachyury* and *Flk1*), (F) ectoderm (*Sox1* and *Pax6*), and (G) endoderm (*Sox17* and *Gata6*) during EB differentiation. Experiments were performed with hMLL1-inducible ESCs. PBS was the solvent control and Dox was added to differentiation medium from day 0 to 6. Data represent average expression (relative to *Gapdh*) ± SEM, n = 3 independent experiments.

colony forming units (CFU) in EBs (McKinney-Freeman et al., 2008). None of the induction regimens altered the peak frequency or kinetics of c-Kit$^+$/Cd41$^+$ cell differentiation (Figures 3A and S3A). However, c-Kit$^+$/Cd41$^+$ cells sorted from hMLL1-induced EBs consistently produced 2-fold more CFU compared with controls (Figure 3B), which reflected a general increase in all colony types (Figures S3B and S3C). This observation was consistent across two additional, independently targeted hMLL1-inducible clones (Figure S3D). Cells harvested at day 7 of the CFU assay exhibited similar surface phenotypes and morphologies (Figures 3C and S3E). The analogous embryo YS-derived EMPs lack B cell potential and are largely Cd16/32$^+$ (Lacaud and Kouskoff, 2017; McGrath et al., 2015), which are also features of our EB-derived EMP-like population (Figure 3C and W.Y., unpublished data). Collectively, these data demonstrate that increasing MLL1 does not influence the production of EMP-like progenitors but selectively increases the hematopoietic potential of the population on a per cell basis.

To determine how hMLL1 induction increases hematopoietic potential, we first considered whether hMLL1 induction affected survival or proliferation of the newly generated EMP-like cells. Sorted day 6 c-Kit$^+$/Cd41$^+$ cells were briefly incubated with 5-bromo-2-deoxyuridine (BrdU) in liquid culture to quantify proliferation in control versus hMLL1-induced populations. No differences were observed in BrdU incorporation, cell-cycle phase

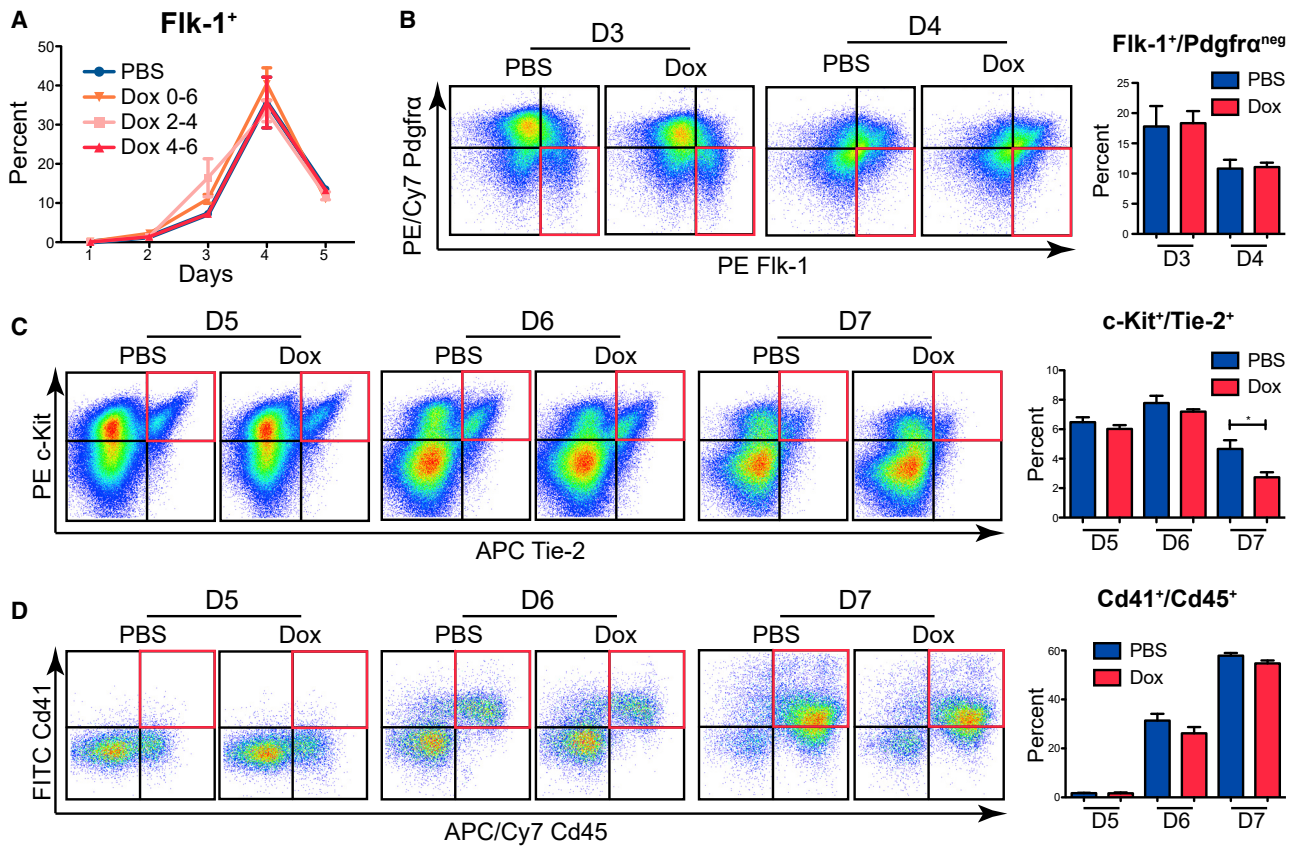

Figure 2. Acquisition of Endothelial and Hematopoietic Markers Occurs Normally upon hMLL1 Induction

(A) Flk-1 surface expression during differentiation of EBs. One representative of three independent experiments is shown as average live-gated, Flk-1$^+$ cells ± SEM of quadruplicate cultures. hMLL1-inducible EBs were treated with vehicle (PBS) or 2 μg/mL doxycycline for indicated days.

(B) Generation of hemangioblast-enriched cells shown by flow cytometry. hMLL1i EBs were treated with solvent (PBS) or doxycycline from day 2 to 4. Quadrant gating is based on single stained controls and the hemangioblast-enriched Flk-1$^+$/Pdgfrα^{neg} population is indicated in red and quantified in the bar graphs (right). Data are representative of two independent experiments and are shown as the average ± SEM of triplicate cultures.

(C and D) (C) Hemogenic endothelium c-Kit$^+$/Tie-2$^+$ and (D) hematopoietic Cd41$^+$/Cd45$^+$ were determined and quantified in the bar graphs. hMLL1i EBs were treated with solvent (PBS) or doxycycline from day 4 to 7. Data are representative of three independent experiments and are shown as averages ± SEM of triplicate cultures.

distribution (Figure 3D), or cells exhibiting sub-2N DNA content (Figure 3E). To investigate whether hMLL1 induction had an impact on self-renewal of this EMP-like population, we determined the serial replating capacity of c-Kit$^+$/Cd41$^+$ hematopoietic progenitors. The initial increase in CFU observed from the induced c-Kit$^+$/Cd41$^+$ population was not sustained upon serial replating (Figure 3F), suggesting the MLL1-dependent increase in CFU occurred during the production of these EMP-like progenitors, rather than within the differentiating population in the CFU assay. Together, these data show that the MLL1-responsive increase in CFU within the c-Kit$^+$/Cd41$^+$ was not explained by selective survival, proliferation, or increase in self-renewal.

To test the impact of MLL1 induction on hematopoietic development *in vivo*, we induced expression of hMLL1 *in utero* from conception (Figure S3F). At E9.5, the percentage of c-Kit$^+$/Cd41$^+$ progenitors in the YS was not affected by hMLL1 induction. However, these cells also produced more CFU on a per cell basis (Figure 3G), similar to the EB observation. We also enumerated hematopoietic cluster cells in the AGM using a whole-mount confocal microscopy technique (Yokomizo et al., 2012). At E10.5, the appearance of c-Kit$^+$/Cd31$^+$/Runx1$^+$ clusters in the ventral wall of the dorsal aorta in the AGM region reflects the emergence of HSCs with definitive potential, whereas c-Kit^{neg}/Cd31$^+$/Runx1$^+$ cells in the same region reflect HE (Jaffredo et al., 1998; North et al., 1999; Yokomizo and Dzierzak,

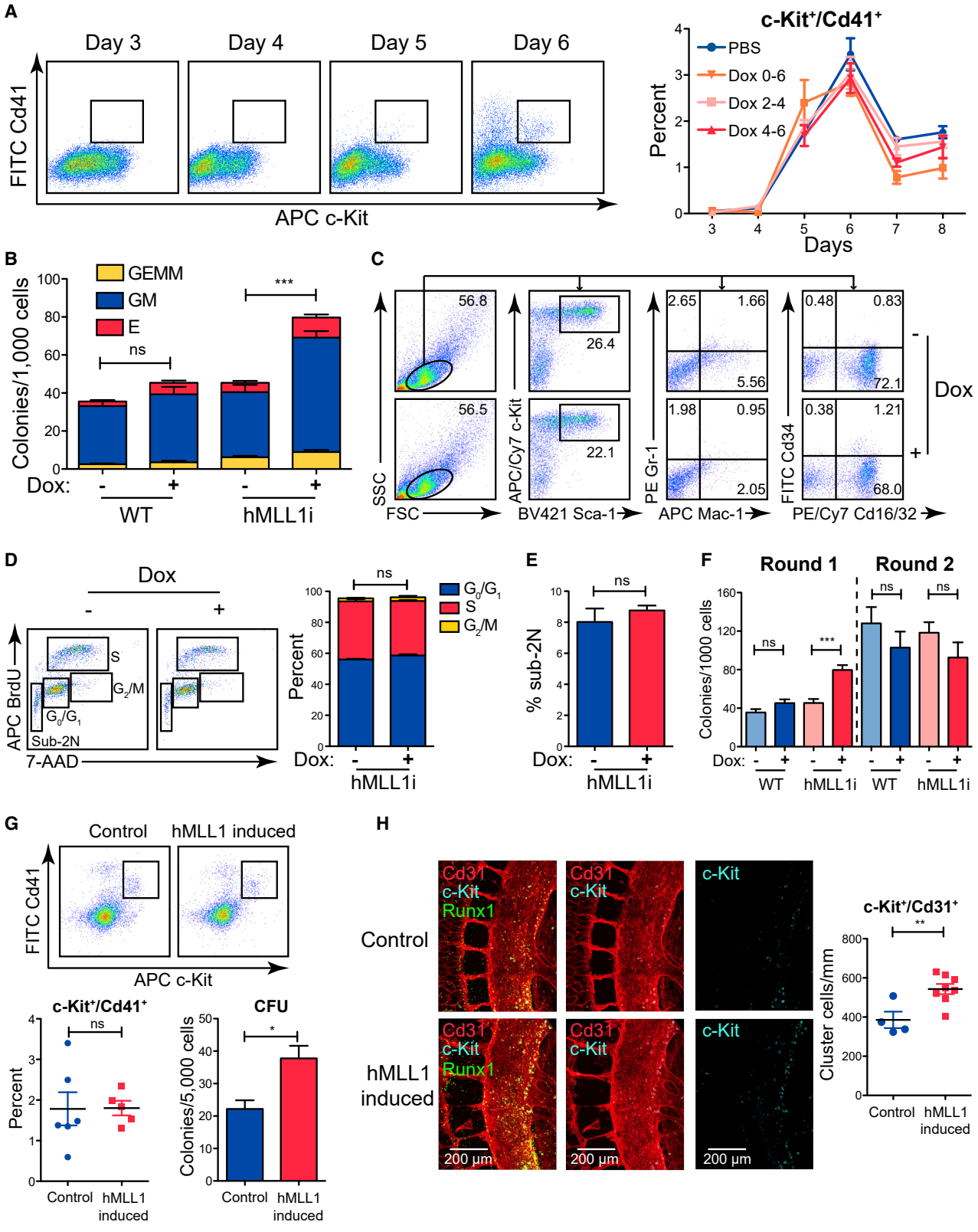

(legend on next page)

2010). In embryos developed with whole-body hMLL1-induction, we observed a significant increase in c-Kit$^+$/Cd31$^+$ cluster cells within five somites of the vitelline artery (Figure 3H), suggesting an enhanced EHT process.

Single-Cell Sequencing Demonstrates that MLL1 Influences the Heterogeneity of the c-Kit$^+$/Cd41$^+$ Population

Despite being the most enriched for hematopoietic potential, the EB day 6 c-Kit$^+$/Cd41$^+$ population is likely not homogeneously committed to the hematopoietic lineage. We hypothesized that MLL1 expression may influence cells within this population that respond to hematopoietic conditions of the CFU assay. We therefore analyzed day 6 c-Kit$^+$/Cd41$^+$ progenitors using single-cell RNA sequencing to determine (1) the heterogeneity of this EMP-like population and (2) whether MLL1 induction changes the composition of this population. Representative pools of sorted c-Kit$^+$/Cd41$^+$ cells from WT or hMLL1-induced day 6 EBs were subjected to single-cell sequencing (Figure S4A). Unsupervised clustering analysis using both WT and hMLL1-induced progenitors suggested three unique populations within the c-Kit$^+$/Cd41$^+$ population (Figures 4A, 4B, S4B, and S4C; the full gene list defining each cluster is shown in Table S1). Cluster 1 (green) was enriched in myeloid and innate immune cell-associated genes such as *Ly6e*, *Ccl3*, *Fcer1g*, *Tyrobp*, and *Cd52* (Figure S4D and Table S1) and enriched the terms "immune system process" and "myeloid leukocyte differentiation" (Figure S4E and Table S1). Cluster 2 (red) was defined by erythroid specific genes such as *Klf1*, *Gata1*, *Hbb-bh1* and enriched the term "erythrocyte differentiation" (Figures S4D and S4E and Table S1). Interestingly, cluster 3 (blue, "HE-like") retained the expression of many endothelial genes, suggesting recent emergence from HE (e.g. *Esam*, *Cdh5*, *Tie1*, *Kdr*) and enriched the terms "vasculature development" and "regulation of angiogenesis" (Figures S4D and S4E and Table S1). *In silico* cell-cycle analysis showed a similar distribution and percentage of S/G_2/M cells within all populations, corroborating our proliferation studies (Figure S4F). This cellular heterogeneity is very similar to that observed in the parallel E9.5 embryo YS c-Kit$^+$/Cd41$^+$/Cd16/32$^+$ population (Kathleen McGrath, Jacquelyn Lillis, and James Palis, personal communication).

To examine the impact of hMLL1 on the distribution of cell types within the c-Kit$^+$/Cd41$^+$ population, we plotted the percentage of each of the three defined clusters in WT versus hMLL1-induced populations (Figure 4C). This analysis showed an increase in myeloid and erythroid populations at the expense of the HE-like population (Figure 4C). We also examined the developmental trajectories of WT and hMLL1-induced samples. Pseudotime analysis with either WT or hMLL1-induced EB progenitors placed the HE-like cluster as a precursor for both erythroid and myeloid/innate immune clusters (Figures 4D and S4G). Collectively, these results suggest that hMLL1 induction reshapes the composition of the c-Kit$^+$/Cd41$^+$ progenitor pool to contain a greater proportion of erythroid- and myeloid-oriented progenitors that may be primed for generating hematopoietic colonies in the CFU assay.

Figure 3. hMLL1 Induction Selectively Affects c-Kit+/Cd41 + Hematopoietic Progenitor Function

(A) Flow cytometry showing the development of c-Kit$^+$/Cd41$^+$ cells. Quantification of representative triplicate cultures is shown in the right panel as the average ± SEM.

(B) CFU assays with 1,000 sorted c-Kit$^+$/Cd41$^+$ cells and colonies scored 7 days later. The bar graph shows data pooled from five independent experiments and presented as averages of triplicate cultures ± SEM. GEMM, granulocyte-erythrocyte-monocyte-megakaryocyte; GM, granulocyte-macrophage; E, erythroid.

(C) Flow cytometry showing similar phenotype of expanded hematopoietic colonies grown on methylcellulose after 7 days.

(D) Cell-cycle status of sorted c-Kit$^+$/Cd41$^+$ cells as determined by BrdU and 7-aminoactinomycin D (7-AAD) staining, quantification is shown in the right panel. Data show one representative experiment of two, bars indicate the average ± SEM of triplicate cultures.

(E) Quantification of 7-AAD low (Sub-2N) cells in the above analyses. Data show one representative experiment of two. Error bar shows the average ± SEM of triplicate cultures.

(F) Serial replating of sorted c-Kit$^+$/Cd41$^+$ progenitors. First round plating was initiated with 1,000 cells. After 7 days, colonies were scored, harvested, and replated using 5,000 cells per dish. Data are normalized to 1,000 input cells. The bar graph shows data pooled from four independent experiments representing triplicate cultures ± SEM.

(G) Flow cytometry showing E9.5 YS c-Kit$^+$/Cd41$^+$ EMPs (top) and quantification (lower left). CFU assays were performed with dissociated E9.5 YS cells and colonies were scored 7 days later. Control embryo genotype = rtTA/+ or hMLL1/+, n = 6; hMLL1-induced embryo genotype = hMLL1/+; rtTA/+, n = 5.

(H) Image and quantification of hematopoietic clusters in E10.5 embryo (34 somite pairs). Left, confocal images show c-Kit (blue), Runx1 (green), and Cd31 (red) expression in the mouse dorsal aorta and vitelline artery region. Right, quantification of hematopoietic cluster (c-Kit$^+$/Cd31$^+$) cells per millimeter of the dorsal aorta. Clusters within five somites centered on the vitelline artery (two somites above, two somites below, and the somite where the vitelline artery connects to the dorsal aorta) were counted. Data represent the average ± SEM, n = 4–8 animals.

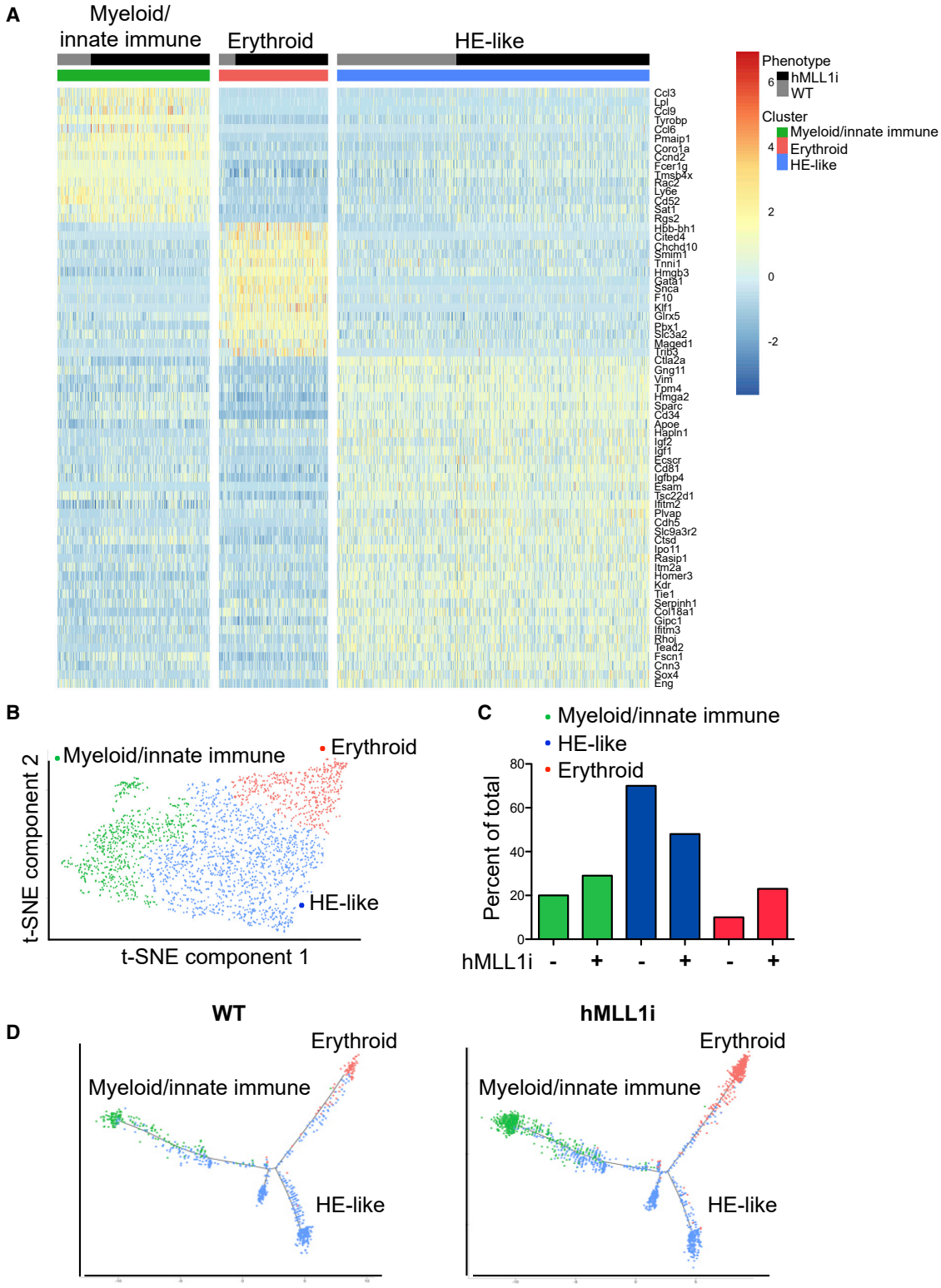

Figure 4. Single-Cell Sequencing Demonstrates that hMLL1 Induction Influences the Heterogeneity of the c-Kit$^+$/Cd41$^+$ Population

(A) Unsupervised hierarchical clustering of gene expression for filtered cells, ordered by average log fold change (see Supplemental Experimental Procedures and Table S1). The top 15 (clusters 1 and 2) or top 37 (cluster 3) genes enriched in each cluster are shown in a heatmap with gene expression represented on a log scale from red to blue (high to low).

(legend continued on next page)

Enhanced Rac/Rho/Integrin Signaling Is a Major Feature of hMLL1-Induced c-Kit$^+$/Cd41$^+$ Progenitors

To understand the mechanisms by which MLL1 induction altered cell fate during hematopoietic progenitor development, we focused on the "HE-like" (cluster 3) cells, since they likely represented the earliest stage of differentiation affected by hMLL1 induction (Figure 4D). Differentially expressed genes comparing WT versus hMLL1-induced cluster 3 cells were identified and subjected to ingenuity pathway analysis (IPA). This approach showed induction of several canonical signaling pathways in the hMLL1-induced samples, for example "Rac signaling," "integrin signaling," and "RhoGDI signaling" (Figure S5A). To confirm and extend these analyses, we performed bulk RNA sequencing using three independently sorted c-Kit$^+$/Cd41$^+$ populations from WT or hMLL1-induced EBs. Principal component analysis indicated that the hMLL1-induced samples cluster by genotype (Figure S5B). Again, IPA analysis using differentially expressed genes from the entire c-Kit$^+$/Cd41$^+$ population recapitulated the results from the single-cell HE-like cluster analysis, showing most significant enrichment of the canonical pathways "Rac signaling," "Rho GTPase signaling," "integrin signaling," and "actin cytoskeleton signaling" (Figures 5A and S5C). These signaling annotations share many genes in common (Lie et al., 2014) (Figure 5B). We confirmed and extended these results using independently sorted samples, including integrins (*Itgb2*, *Itgal*, *Itga4*), Rac/Rho small GTPases (*Rac1*, *Rac2*, *Rhoa*), kinases (*Akt1*, *Pi3kcd*), regulatory subunits or cytoskeleton proteins (*Myl12a/b*, *Actb*, *Arp3*) (Figures 5C and S5D). Immunofluorescence staining of F-actin showed increased spontaneous cell spreading in hMLL1-induced Cd41-enriched progenitors when incubated on fibronectin, suggesting enhanced propensity for re-organization of actin filaments upon adhesion (Figure 5D). Together, these results demonstrate that hMLL1 induction activates a Rac/Rho/integrin cellular signaling state and enhances integrin-mediated adhesion and cytoskeletal rearrangement.

hMLL1 Induction Specifically Promotes Integrin-Mediated Cell Adhesion, Increasing Hematopoietic Potential

To test the functional impact of enhanced Rac/Rho/integrin signaling pathways, we first tested cell-surface expression of candidate integrins. Among all MLL1-induced candidates from RNA sequencing analysis, we only observed a significant increase in the percentage of Cd49d+ (encoded by *Itga4*, a subunit of Vla4) cells within the c-Kit$^+$/Cd41$^+$ day 6 EB cell population (Figure 6A). Surface expression of the other subunit of Vla4, Cd29 (encoded by *Itgb1*) and other expressed integrins (Cd11a, encoded by *ItgaL*; Cd18, encoded by *Itgb2*) did not change upon hMLL1 induction (Figure S6A). To test whether hMLL1-induced progenitors exhibited an increase in an integrin-mediated function, we allowed cells to adhere to the integrin ligand-coated surfaces and tested baseline adhesion and the effect on hematopoietic potential (Figure 6B). hMLL1-induced progenitors consistently exhibited increased adhesion to the Vla4 ligands fibronectin and Vcam1 relative to control progenitors (Figure 6C). This observation was reproduced with additional independent hMLL1-inducible ESC clones (Figure S6B). To investigate the functional outcome of engaging Vla4, we cultured Cd41-enriched progenitors on fibronectin-coated wells for 24 h then transferred all cells to the CFU assay (Figure 6D). Although fibronectin binding did not influence the CFU of WT cells, it further increased CFUs from hMLL1-induced cells (Figures 6D and S6C). To test if this MLL1-dependent CFU increase occurs through Rac-mediated signaling, we treated hMLL1-induced cells briefly with a Rac1 specific inhibitor (NSC23766) and then performed CFU assays. While WT cells did not exhibit changes in CFU frequency, use of the Rac inhibitor on hMLL1-induced cells significantly decreased CFU frequencies, bringing them back to levels observed in WT untreated cells (Figures 6D and S6D). These data collectively suggest that the enhanced signaling state produced by hMLL1 induction is Rac1-dependent and increases responsiveness to Vla4 ligands, resulting in enhanced hematopoietic commitment from the transitional c-Kit$^+$/Cd41$^+$ population.

DISCUSSION

Here, we present a model system in which increasing MLL1 protein levels within a physiologically reasonable range can be achieved and show that this perturbation selectively increases hematopoietic potential during a transition from endothelial to hematopoietic fate. The approach used here has been very useful for testing the effect of consistent and physiologic overexpression of several transcription factors including Scl, Cdx4, Hoxb4, Mix1, and Notch1 (Ismailoglu et al., 2008; Kubo et al., 2005; Kyba

(B) T-distributed stochastic neighbor embedding (t-SNE) plot of WT (KH2) and hMLL1-induced c-Kit$^+$/Cd41$^+$ cells colored by clusters according to (A).

(C) Proportion of cells within each cluster is shown in the bar graph.

(D) WT or hMLL1-induced cells are arranged by pseudotime axis (see Supplemental Experimental Procedures) with cells colored by clusters according to (A).

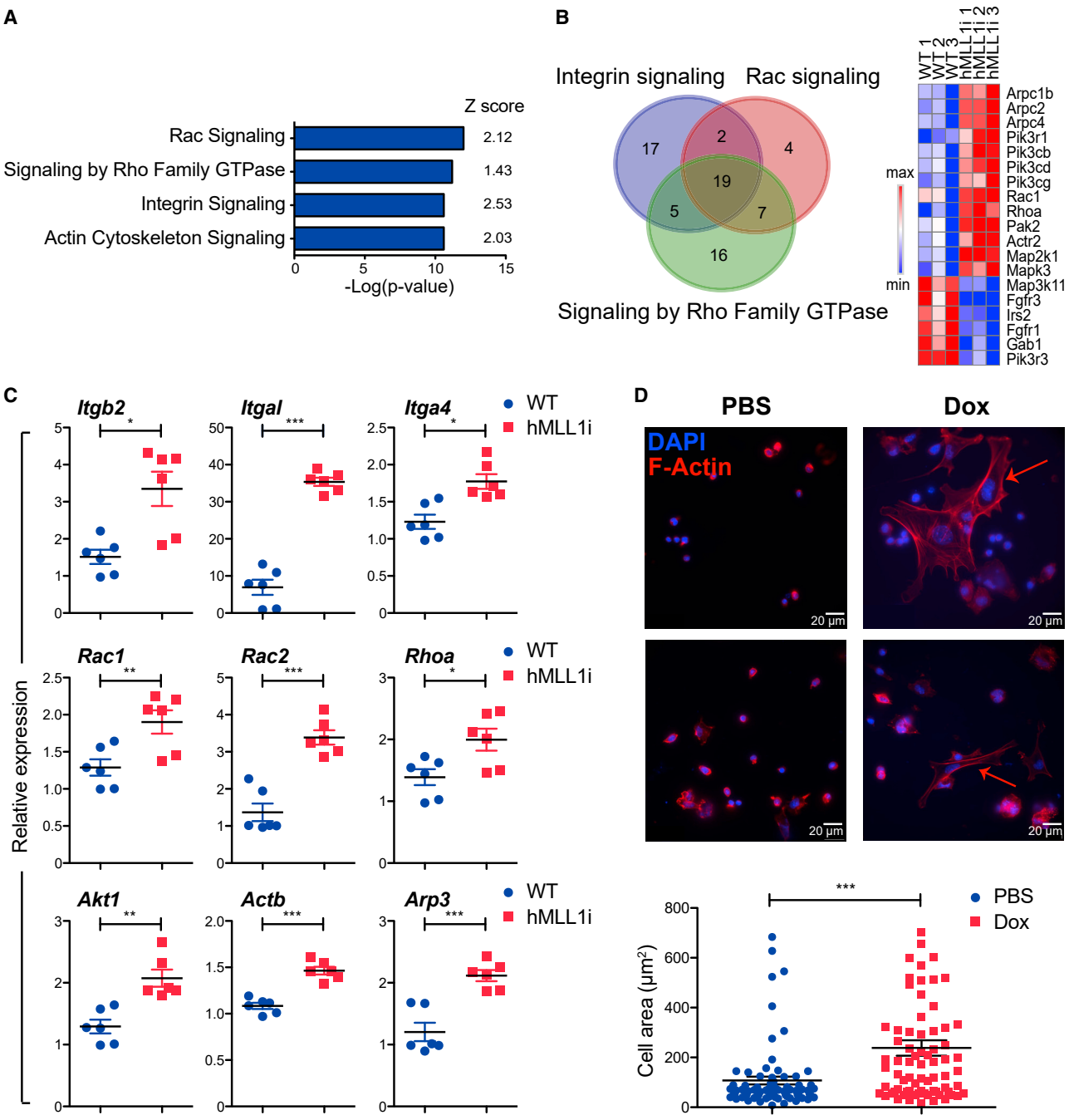

Figure 5. Genetic Programs and Molecular Pathways Associated with hMLL1 Induction

(A) IPA analysis to show the top pathways (by p value) regulated by hMLL1 induction.

(B) Venn diagram displays overlap of the top three major signaling pathways by p value affected by hMLL1 induction. Expression heatmap of overlap genes is shown on the right.

(C) Quantitative RT-PCR validates the upregulation of Rac/Rho/integrin signaling in hMLL1-induced c-Kit$^+$/Cd41$^+$ cells. Data show expression relative to *Gapdh* determined by qRT-PCR from three independently sorted samples ± SEM.

(D) Representative images showing F-actin visualized with rhodamine-conjugated phalloidin in Cd41$^+$ enriched cells ± hMLL1 induction. Arrows indicate spreading actin stress fibers. At least 80 cells in each sample were quantified, and cell areas were measured using ImageJ software. Data represent the average ± SEM from two independent experiments.

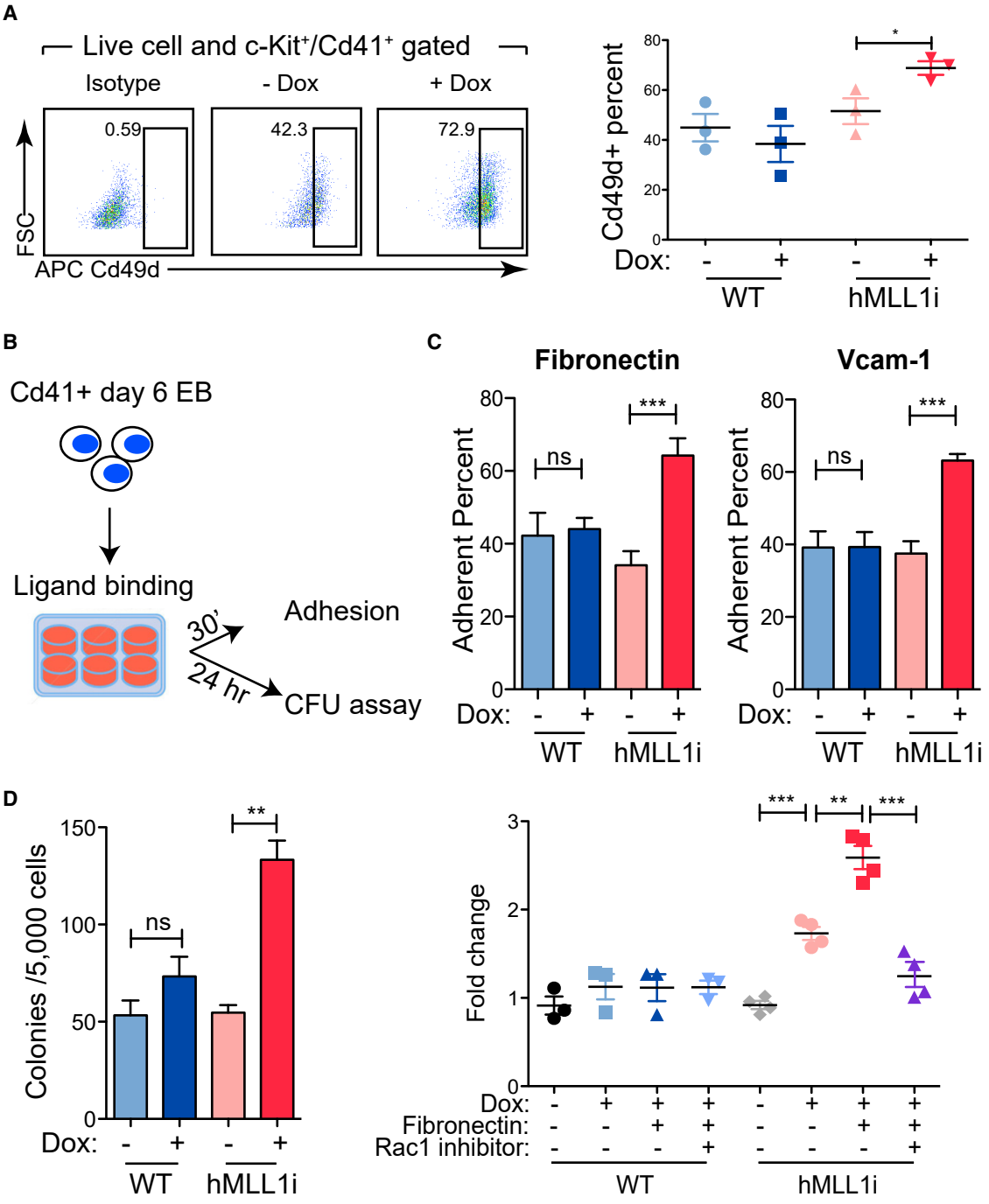

Figure 6. hMLL1 Induction Specifically Promotes Integrin-Mediated Cell Adhesion and Further Expands CFU

(A) Flow cytometry to detect Cd49d expression in c-Kit$^+$/Cd41$^+$ gated EB cells. Quantification of one representative experiment from three independent differentiation experiments is shown on the right. Data show the average ± SEM, n = triplicate cultures.

(B) Experimental procedure to test integrin function. Day 6 EB Cd41$^+$ enriched WT or hMLL1-inducible cells were cultured on integrin ligand (fibronectin or Vcam1)-coated plates for the indicated time and tested for adhesion or CFU content.

(C) Cell adhesion of Cd41$^+$ enriched progenitors to fibronectin and Vcam1. Data are representative of four independent experiments and presented as the average of triplicate cultures ± SEM.

(D) CFU assay using sorted Cd41$^+$ EB progenitors following 24 h adhesion. Adherent cells were harvested with dissociation buffer and pooled with remaining suspension cells, then counted for CFU assay. Left: both hMLL1-inducible and WT cells were adhered to fibronectin

(legend continued on next page)

et al., 2002; McKinney-Freeman et al., 2008; Meier-Stiegen et al., 2010; Wang et al., 2005; Willey et al., 2006). In contrast to the effect of hMLL1 induction, Cdx4 or Hoxb4 overexpression increases c-Kit$^+$/Cd41$^+$ hematopoietic progenitors at an earlier stage, promoting formation of HE and subsequently, hematopoietic potential (Teichweyde et al., 2018; Wang et al., 2005). While inducing hMLL1 apparently does not numerically affect HE or increase c-Kit$^+$/Cd41$^+$ progenitors, it reshapes the composition of this population, resulting in enhanced hematopoietic potential. Interestingly, we also observe an increase in hematopoietic clusters from HE in the dorsa aorta of hMLL1-induced E10.5 embryos, suggesting that hMLL1 plays a parallel role in a distinct hemogenic endothelial site *in vivo*. The specific impact of MLL1 induction may be due to the regulation of a yet undefined network regulating Rac1 activity, integrin-mediated adhesion, and cytoskeletal rearrangement during the EHT process.

The application of single-cell RNA sequencing in this setting enabled us to investigate the heterogeneity of a murine EB-derived EMP-like hematopoietic progenitor pool, which has not yet been addressed. Comparative analysis of our *in vitro* day 6 c-Kit$^+$/Cd41$^+$ EMP-like progenitor with the E9.5 *in vivo* YS EMP (McGrath et al., 2015) single-cell sequencing data showed a very similar composition, including a residual HE-like population, an erythroid and a myeloid/innate immune population (Kathleen McGrath, Jacquelyn Lillis, and James Palis, personal communication). The similarities in transcriptome-defined populations *in vivo* and *in vitro* underscore the relevance of the ESC system for dissecting sequential developmental stages of hematopoiesis. The presence of a residual HE-like gene expression signature is consistent with the observation that the onset of hematopoietic potential commences with Cd41 expression within a hemogenic endothelial population (Lancrin et al., 2009; McGrath et al., 2015), thus the c-Kit$^+$/Cd41$^+$ population likely represents an asynchronous pool of cells with varying degrees of "memory" of hemogenic endothelial identity. We interpret the single-cell transcriptome data to suggest that hMLL1 induction alters the composition of the EMP-like progenitor pool, resulting in either more efficient commitment to the hematopoietic lineages at the expense of the HE-like population, or that hMLL1 induction accelerated kinetics of departure from an HE-like state toward the myeloid- and erythroid-primed progenitors. Given our observations that hMLL1 induction does not increase the c-Kit$^+$/Cd41$^+$ population, as well as the similarity of the kinetics developing hemogenic populations, it seems more likely that hMLL1 induction promotes hematopoiesis by driving more efficient commitment to multilineage hematopoietic fates.

A very surprising finding was the fact that hMLL1 induction did not affect *Hox* cluster gene expression. The generally low expression levels of *Hoxa-d* clusters in EB-derived hematopoietic progenitors has been noted by others (Dou et al., 2016; Ng et al., 2016). This feature of EB-derived and YS-derived progenitors may underlie their inability to generate definitive HSCs since the parallel or immunophenotypically similar fetal liver progenitors can express much higher *Hox* levels (Dou et al., 2016). We speculate that the acquisition of a *Hoxa* signature may need additional sequence-specific transcriptional inputs (e.g., retinoic acid signaling) (Dou et al., 2016), while MLL1 itself is not capable of such induction, consistent with the role of Trithorax as a maintenance factor rather than inducer of gene expression (Schuettengruber et al., 2011). In fact, preliminary data suggest that *Hoxa* induction by retinoic acid receptor agonists is sustained more efficiently in the presence of induced hMLL1 (W.Y., unpublished data).

Interestingly, induction of hMLL1 does not lead to leukemic transformation as with MLL fusion oncoproteins in other cellular settings. Recent work by Bueno et al. demonstrates that ectopic expression of MLL-AF4 is not sufficient to induce leukemic transformation in human ESC-derived hematopoietic cells (Bueno et al., 2012, 2019), consistent with our observation that inducing MLL-ENL does not transform ES-derived hematopoietic progenitors (W.Y. and D.B., unpublished data). These findings raise questions about the responsiveness of EMP-like populations to transformation, specifically by oncogenes that may require induction of a *Hox* program. The lack of or limited *Hox* induction in hMLL1-induced cultures or the distinct dynamic pattern (Spencer et al., 2015; Zeisig et al., 2004) in MLL fusion transduced EBs may represent a hurdle that restrains cell growth or transformation. Overcoming this hurdle may require developmental context and *Hox* regulators in addition to MLL1. Defining exact window of development and mechanisms of *Hox* locus responsiveness may shed light on the cell of origin and pediatric association of *MLL1* translocations (Barrett et al., 2016).

In this study, we identified Rac/Rho/integrin signaling as a major axis activated by hMLL1 induction within the EMP-like population of developing EBs. hMLL1 induction resulted in increased *Itga4*, *Itgal*, and *Itgb2* transcripts and

fragment and then followed by CFU assay. One representative experiment of three is shown as the average ± SEM, n = 3 triplicate cultures. Right: quantification of CFU fold changes with Dox, fibronectin fragment, or Rac1 inhibitor (NSC23766, 10 μM). The graph show data pooled from 3 to 4 independent experiments (n = 3 for WT; n = 4 for hMLL1i, with each data point representing the average of triplicate cultures) representing the overall average ± SEM.

increased Cd49d surface expression. hMLL1 induction also promotes integrin-mediated cell adhesion and further activation of integrin signaling through Vla4, resulting in enhanced CFU from this EMP-like population. Several previous studies have implicated the Rac/Rho/integrin axis as limiting for hematopoietic development and homeostasis. First, the Cd49d$^+$ fraction of ESC-derived endothelium is enriched in both primitive and definitive hematopoietic progenitor activity (Shinoda et al., 2007). Second, Rac1 activation during early embryonic hematopoiesis in the dorsal aorta, as well as Rac2 and Cdc42 activation in Lin^{neg}/c-Kit$^+$/Sca-1$^+$ HSPCs, is associated with Vla4-mediated adhesion, migration, engraftment, and survival of HSPCs (Ghiaur et al., 2008; Yang et al., 2001). Interestingly, studies identifying Runx1 target genes in hemogenic endothelia of the embryo or in EBs also revealed integrin signaling, Rho signaling, cytoskeletal organization, and cell adhesion as enriched pathways regulated by Runx1 (Gao et al., 2018; Lie et al., 2014). The effect of Runx1 induction has been proposed to be in part through direct regulation of the integrin Cd61 (*Itgb3*) (Lie et al., 2014). The cause of widespread Rac/Rho activation in hMLL1-induced EMP-like progenitors is unclear but may reflect a complex combination of direct and indirect effects of increasing MLL1 levels. Since we observe downregulation of several RhoGEFs, it is also possible that compensatory upregulation of the Rac/Rho pathways results in the more active adhesion phenotype in MLL1-induced progenitors and could account for the greater number of hematopoietic cells in the aortic clusters. Collectively, our data underscore the impact of integrin/Rac/Rho signaling in the EHT process, and that Runx1 and MLL1 may both regulate this critical step in parallel.

In summary, utilizing this physiologic MLL1-inducible model system revealed an unanticipated connection between MLL1 and integrin-mediated signaling that appears to enhance the efficiency of EHT. Whether these pathways are conserved in the later waves of hematopoiesis in the embryo and adult, and whether they can collaborate with other signals for more efficient production of HSPCs, will be important future questions.

EXPERIMENTAL PROCEDURES

ESC Culture and Differentiation

ESCs were maintained on embryonic fibroblasts using standard conditions (Ernst et al., 2004b). For *in vitro* differentiation, single-cell suspensions from dissociated ESC cultures were seeded at 10,000–20,000 cells/mL in Petri dishes (Fisher) with orbital rotation (50 rpm, Labnet Orbit 1000). The differentiation medium was Iscove's modified Dulbecco's medium (Mediatech) containing 15% fetal bovine serum (Gibco), 2 mM L-glutamine (Mediatech), 1% penicillin/streptomycin (Mediatech), 200 μg/mL holo bovine transferrin (Millipore), 4.5 × 10^{-4} M monothioglycerol (Sigma) and 50 μg/mL ascorbic acid (Sigma). Doxycycline (Enzo Life Sciences) was added to the differentiation medium at 1–2 μg/mL for the times indicated in each figure legend.

Flow Cytometry, Cell Isolation, and Sorting

EBs were dissociated with collagenase (0.8 U/mL, Sigma) and dispase I (2 mg/mL, Sigma) and then incubated with the indicated antibodies (Biolegend or eBiosciences). Stained cells were analyzed or sorted using an LSR Fortessa or FACSAria Fusion, respectively (BD Biosciences). Gating was based on either single color or isotype control staining. Enrichment was performed using Miltenyi Cd41 magnetic beads. Flow cytometry data were analyzed using FlowJo software (TreeStar).

Single-Cell Sequencing, RNA Sequencing, and Bioinformatics

Single-cell RNA sequencing was performed with singlet-gated, DAPI-negative, c-Kit$^+$/Cd41$^+$ cells from day 6 EBs sorted using a FACSAria Fusion. Cell purity was determined by post-sort re-analysis and was typically >90% (Figure S4A). Approximately 4,000 sorted cells were used to generate libraries and sequenced by the University of Colorado Cancer Center Genomics and Microarray core facility. Bulk RNA sequencing was performed using sorted c-Kit$^+$/Cd41$^+$ pools of cells from WT (KH2) or hMLL1-inducible EBs incubated with doxycycline from day 4 to day 6. Three separate differentiation experiments were performed with WT (KH2) and hMLL1i differentiated in parallel. Detailed sequencing data analysis and methods can be found in Supplemental Experimental Procedures.

Statistical Analyses

Significance was analyzed in all studies using unpaired Student's t tests and standard error of the mean (SEM) with *$p < 0.05$, **$p < 0.01$, ***$p < 0.001$ considered significant unless otherwise indicated in the figure legends. GraphPad Prism or Microsoft Excel software was used to perform the statistical calculations.

ACCESSION NUMBERS

The sequencing data are available at the Gene Expression Omnibus under GEO: GSE129169 and GSE129170.

SUPPLEMENTAL INFORMATION

Supplemental Information can be found online at https://doi.org/10.1016/j.stemcr.2019.12.009.

AUTHOR CONTRIBUTIONS

W.Y. designed and performed most experiments, analyzed data, and co-wrote the manuscript; G.D.T., K.L.J., A.E.G., K.R., and J.H. performed or supervised bioinformatics analyses; E.D.H performed experiments; N.A.S. edited the manuscript; D.B. contributed expertise and reagents; P.E. designed and supervised the research, analyzed data, and co-wrote the manuscript.

CONFLICTS OF INTEREST

P.E. has Amgen stock and has consulted for Servier Oncology.

ACKNOWLEDGMENTS

We thank our lab members, Hanna Mikkola, Marie-Dominique Filippi, and James Palis for critical review. We thank Claire Wingert and Louisa Wingert for preparing the GAL4 fusion constructs, and Gerd Stein for help generating targeted ESC clones. We are grateful to Alan Cantor for reagents and Kyunghee Choi, Ruben Kapur, Bertie Göttgens and Jacquelyn Lillis for critical advice and discussion, and the University of Colorado Cancer Center Microarray and Genomics Core for excellent support. This work was funded by R21OD019716, R21AI112143673, P30CA046934 and by a pilot grant from the RNA Bioscience Initiative, University of Colorado School of Medicine.

Received: June 17, 2019
Revised: December 12, 2019
Accepted: December 17, 2019
Published: January 16, 2020

REFERENCES

Barrett, N.A., Malouf, C., Kapeni, C., Bacon, W.A., Giotopoulos, G., Jacobsen, S.E.W., Huntly, B.J., and Ottersbach, K. (2016). Mll-AF4 confers enhanced self-renewal and lymphoid potential during a restricted window in development. Cell Rep. *16*, 1039–1054.

Beard, C., Hochedlinger, K., Plath, K., Wutz, A., and Jaenisch, R. (2006). Efficient method to generate single-copy transgenic mice by site-specific integration in embryonic stem cells. Genesis *44*, 23–28.

Bertrand, J.Y., Chi, N.C., Santoso, B., Teng, S., Stainier, D.Y., and Traver, D. (2010). Haematopoietic stem cells derive directly from aortic endothelium during development. Nature *464*, 108–111.

Bertrand, J.Y., Jalil, A., Klaine, M., Jung, S., Cumano, A., and Godin, I. (2005). Three pathways to mature macrophages in the early mouse yolk sac. Blood *106*, 3004–3011.

Boisset, J.C., van Cappellen, W., Andrieu-Soler, C., Galjart, N., Dzierzak, E., and Robin, C. (2010). In vivo imaging of haematopoietic cells emerging from the mouse aortic endothelium. Nature *464*, 116–120.

Bueno, C., Calero-Nieto, F.J., Wang, X., Valdes-Mas, R., Gutierrez-Aguera, F., Roca-Ho, H., Ayllon, V., Real, P.J., Arambile, D., Espinosa, L., et al. (2019). Enhanced hemato-endothelial specification during human embryonic differentiation through developmental cooperation between AF4-MLL and MLL-AF4 fusions. Haematologica *104*, 1189–1201.

Bueno, C., Montes, R., Melen, G.J., Ramos-Mejia, V., Real, P.J., Ayllon, V., Sanchez, L., Ligero, G., Gutierrez-Aranda, I., Fernandez, A.F., et al. (2012). A human ESC model for MLL-AF4 leukemic fusion gene reveals an impaired early hematopoietic-endothelial specification. Cell Res. *22*, 986–1002.

Choi, K., Kennedy, M., Kazarov, A., Papadimitriou, J.C., and Keller, G. (1998). A common precursor for hematopoietic and endothelial cells. Development *125*, 725–732.

Denissov, S., Hofemeister, H., Marks, H., Kranz, A., Ciotta, G., Singh, S., Anastassiadis, K., Stunnenberg, H.G., and Stewart, A.F. (2014). Mll2 is required for H3K4 trimethylation on bivalent promoters in embryonic stem cells, whereas Mll1 is redundant. Development *141*, 526–537.

Ditadi, A., Sturgeon, C.M., and Keller, G. (2017). A view of human haematopoietic development from the Petri dish. Nat. Rev. Mol. Cell Biol. *18*, 56–67.

Dorrance, A.M., Liu, S., Yuan, W., Becknell, B., Arnoczky, K.J., Guimond, M., Strout, M.P., Feng, L., Nakamura, T., Yu, L., et al. (2006). Mll partial tandem duplication induces aberrant Hox expression in vivo via specific epigenetic alterations. J. Clin. Invest. *116*, 2707–2716.

Dou, D.R., Calvanese, V., Sierra, M.I., Nguyen, A.T., Minasian, A., Saarikoski, P., Sasidharan, R., Ramirez, C.M., Zack, J.A., Crooks, G.M., et al. (2016). Medial HOXA genes demarcate haematopoietic stem cell fate during human development. Nat. Cell Biol. *18*, 595–606.

Dzierzak, E., and Bigas, A. (2018). Blood development: hematopoietic stem cell dependence and independence. Cell Stem Cell *22*, 639–651.

Dzierzak, E., and Speck, N.A. (2008). Of lineage and legacy: the development of mammalian hematopoietic stem cells. Nat. Immunol. *9*, 129–136.

Eilken, H.M., Nishikawa, S., and Schroeder, T. (2009). Continuous single-cell imaging of blood generation from haemogenic endothelium. Nature *457*, 896–900.

Ernst, P., Fisher, J.K., Avery, W., Wade, S., Foy, D., and Korsmeyer, S.J. (2004a). Definitive hematopoiesis requires the mixed-lineage leukemia gene. Dev. Cell *6*, 437–443.

Ernst, P., Mabon, M., Davidson, A.J., Zon, L.I., and Korsmeyer, S.J. (2004b). An Mll-dependent Hox program drives hematopoietic progenitor expansion. Curr. Biol. *14*, 2063–2069.

Frame, J.M., Fegan, K.H., Conway, S.J., McGrath, K.E., and Palis, J. (2016). Definitive Hematopoiesis in the yolk sac emerges from wnt-responsive hemogenic endothelium independently of circulation and arterial identity. Stem Cells *34*, 431–444.

Gao, L., Tober, J., Gao, P., Chen, C., Tan, K., and Speck, N.A. (2018). RUNX1 and the endothelial origin of blood. Exp. Hematol. *68*, 2–9.

Ghiaur, G., Ferkowicz, M.J., Milsom, M.D., Bailey, J., Witte, D., Cancelas, J.A., Yoder, M.C., and Williams, D.A. (2008). Rac1 is essential for intraembryonic hematopoiesis and for the initial seeding of fetal liver with definitive hematopoietic progenitor cells. Blood *111*, 3313–3321.

Gritz, E., and Hirschi, K.K. (2016). Specification and function of hemogenic endothelium during embryogenesis. Cell. Mol. Life Sci. *73*, 1547–1567.

Ismailoglu, I., Yeamans, G., Daley, G.Q., Perlingeiro, R.C., and Kyba, M. (2008). Mesodermal patterning activity of SCL. Exp. Hematol. *36*, 1593–1603.

Jaffredo, T., Gautier, R., Eichmann, A., and Dieterlen-Lievre, F. (1998). Intraaortic hemopoietic cells are derived from endothelial cells during ontogeny. Development *125*, 4575–4583.

Joh, T., Kagami, Y., Yamamoto, K., Segawa, T., Takizawa, J., Takahashi, T., Ueda, R., and Seto, M. (1996). Identification of MLL and chimeric MLL gene products involved in 11q23 translocation and possible mechanisms of leukemogenesis by MLL truncation. Oncogene *13*, 1945–1953.

Jude, C.D., Climer, L., Xu, D., Artinger, E., Fisher, J.K., and Ernst, P. (2007). Unique and independent roles for MLL in adult hematopoietic stem cells and progenitors. Cell Stem Cell *1*, 324–337.

Kataoka, H., Hayashi, M., Nakagawa, R., Tanaka, Y., Izumi, N., Nishikawa, S., Jakt, M.L., Tarui, H., and Nishikawa, S. (2011). Etv2/ER71 induces vascular mesoderm from Flk1+PDGFRalpha+ primitive mesoderm. Blood *118*, 6975–6986.

Kattman, S.J., Huber, T.L., and Keller, G.M. (2006). Multipotent flk-1+ cardiovascular progenitor cells give rise to the cardiomyocyte, endothelial, and vascular smooth muscle lineages. Dev. Cell *11*, 723–732.

Keller, G. (2005). Embryonic stem cell differentiation: emergence of a new era in biology and medicine. Genes Dev. *19*, 1129–1155.

Kennedy, M., D'Souza, S.L., Lynch-Kattman, M., Schwantz, S., and Keller, G. (2007). Development of the hemangioblast defines the onset of hematopoiesis in human ES cell differentiation cultures. Blood *109*, 2679–2687.

Krivtsov, A.V., and Armstrong, S.A. (2007). MLL translocations, histone modifications and leukaemia stem-cell development. Nat. Rev. Cancer *7*, 823–833.

Kubo, A., Chen, V., Kennedy, M., Zahradka, E., Daley, G.Q., and Keller, G. (2005). The homeobox gene HEX regulates proliferation and differentiation of hemangioblasts and endothelial cells during ES cell differentiation. Blood *105*, 4590–4597.

Kyba, M., Perlingeiro, R.C., and Daley, G.Q. (2002). HoxB4 confers definitive lymphoid-myeloid engraftment potential on embryonic stem cell and yolk sac hematopoietic progenitors. Cell *109*, 29–37.

Lacaud, G., and Kouskoff, V. (2017). Hemangioblast, hemogenic endothelium, and primitive versus definitive hematopoiesis. Exp. Hematol. *49*, 19–24.

Lancrin, C., Sroczynska, P., Stephenson, C., Allen, T., Kouskoff, V., and Lacaud, G. (2009). The haemangioblast generates haematopoietic cells through a haemogenic endothelium stage. Nature *457*, 892–895.

Lie, A.L.M., Marinopoulou, E., Li, Y., Patel, R., Stefanska, M., Bonifer, C., Miller, C., Kouskoff, V., and Lacaud, G. (2014). RUNX1 positively regulates a cell adhesion and migration program in murine hemogenic endothelium prior to blood emergence. Blood *124*, e11–20.

Liu, H., Cheng, E.H., and Hsieh, J.J. (2007). Bimodal degradation of MLL by SCFSkp2 and APCCdc20 assures cell cycle execution: a critical regulatory circuit lost in leukemogenic MLL fusions. Genes Dev. *21*, 2385–2398.

Lugus, J.J., Park, C., Ma, Y.D., and Choi, K. (2009). Both primitive and definitive blood cells are derived from Flk-1+ mesoderm. Blood *113*, 563–566.

Lux, C.T., Yoshimoto, M., McGrath, K., Conway, S.J., Palis, J., and Yoder, M.C. (2008). All primitive and definitive hematopoietic progenitor cells emerging before E10 in the mouse embryo are products of the yolk sac. Blood *111*, 3435–3438.

McGrath, K.E., Frame, J.M., Fegan, K.H., Bowen, J.R., Conway, S.J., Catherman, S.C., Kingsley, P.D., Koniski, A.D., and Palis, J. (2015). Distinct sources of hematopoietic progenitors emerge before HSCs and provide functional blood cells in the mammalian embryo. Cell Rep. *11*, 1892–1904.

McKinney-Freeman, S.L., Lengerke, C., Jang, I.H., Schmitt, S., Wang, Y., Philitas, M., Shea, J., and Daley, G.Q. (2008). Modulation of murine embryonic stem cell-derived CD41+c-kit+ hematopoietic progenitors by ectopic expression of Cdx genes. Blood *111*, 4944–4953.

McMahon, K.A., Hiew, S.Y., Hadjur, S., Veiga-Fernandes, H., Menzel, U., Price, A.J., Kioussis, D., Williams, O., and Brady, H.J. (2007). Mll has a critical role in fetal and adult hematopoietic stem cell self-renewal. Cell Stem Cell *1*, 338–345.

Meier-Stiegen, F., Schwanbeck, R., Bernoth, K., Martini, S., Hieronymus, T., Ruau, D., Zenke, M., and Just, U. (2010). Activated Notch1 target genes during embryonic cell differentiation depend on the cellular context and include lineage determinants and inhibitors. PLoS One *5*, e11481.

Mishra, B.P., Zaffuto, K.M., Artinger, E.L., Org, T., Mikkola, H.K., Cheng, C., Djabali, M., and Ernst, P. (2014). The histone methyltransferase activity of MLL1 is dispensable for hematopoiesis and leukemogenesis. Cell Rep. *7*, 1239–1247.

Ng, E.S., Azzola, L., Bruveris, F.F., Calvanese, V., Phipson, B., Vlahos, K., Hirst, C., Jokubaitis, V.J., Yu, Q.C., Maksimovic, J., et al. (2016). Differentiation of human embryonic stem cells to HOXA(+) hemogenic vasculature that resembles the aorta-gonad-mesonephros. Nat. Biotechnol. *34*, 1168–1179.

North, T., Gu, T.L., Stacy, T., Wang, Q., Howard, L., Binder, M., Marin-Padilla, M., and Speck, N.A. (1999). Cbfa2 is required for the formation of intra-aortic hematopoietic clusters. Development *126*, 2563–2575.

Palis, J., Robertson, S., Kennedy, M., Wall, C., and Keller, G. (1999). Development of erythroid and myeloid progenitors in the yolk sac and embryo proper of the mouse. Development *126*, 5073–5084.

Poppe, B., Vandesompele, J., Schoch, C., Lindvall, C., Mrozek, K., Bloomfield, C.D., Beverloo, H.B., Michaux, L., Dastugue, N., Herens, C., et al. (2004). Expression analyses identify MLL as a prominent target of 11q23 amplification and support an etiologic role for MLL gain of function in myeloid malignancies. Blood *103*, 229–235.

Robertson, S.M., Kennedy, M., Shannon, J.M., and Keller, G. (2000). A transitional stage in the commitment of mesoderm to hematopoiesis requiring the transcription factor SCL/tal-1. Development *127*, 2447–2459.

Rowe, R.G., Mandelbaum, J., Zon, L.I., and Daley, G.Q. (2016). Engineering hematopoietic stem cells: lessons from development. Cell Stem Cell *18*, 707–720.

Schuettengruber, B., Martinez, A.M., Iovino, N., and Cavalli, G. (2011). Trithorax group proteins: switching genes on and keeping them active. Nat. Rev. Mol. Cell Biol. *12*, 799–814.

Shalaby, F., Ho, J., Stanford, W.L., Fischer, K.D., Schuh, A.C., Schwartz, L., Bernstein, A., and Rossant, J. (1997). A requirement for Flk1 in primitive and definitive hematopoiesis and vasculogenesis. Cell *89*, 981–990.

Shinoda, G., Umeda, K., Heike, T., Arai, M., Niwa, A., Ma, F., Suemori, H., Luo, H.Y., Chui, D.H., Torii, R., et al. (2007). alpha4-Integrin(+) endothelium derived from primate embryonic stem cells generates primitive and definitive hematopoietic cells. Blood *109*, 2406–2415.

Spencer, D.H., Young, M.A., Lamprecht, T.L., Helton, N.M., Fulton, R., O'Laughlin, M., Fronick, C., Magrini, V., Demeter, R.T., Miller, C.A., et al. (2015). Epigenomic analysis of the HOX gene loci reveals mechanisms that may control canonical expression patterns in AML and normal hematopoietic cells. Leukemia *29*, 1279–1289.

Tang, G., DiNardo, C., Zhang, L., Ravandi, F., Khoury, J.D., Huh, Y.O., Muzzafar, T., Medeiros, L.J., Wang, S.A., and Bueso-Ramos, C.E. (2015). MLL gene amplification in acute myeloid leukemia and myelodysplastic syndromes is associated with characteristic clinicopathological findings and TP53 gene mutation. Hum. Pathol. *46*, 65–73.

Teichweyde, N., Kasperidus, L., Carotta, S., Kouskoff, V., Lacaud, G., Horn, P.A., Heinrichs, S., and Klump, H. (2018). HOXB4 promotes hemogenic endothelium formation without perturbing endothelial cell development. Stem Cell Rep. *10*, 875–889.

Tober, J., Koniski, A., McGrath, K.E., Vemishetti, R., Emerson, R., de Mesy-Bentley, K.K., Waugh, R., and Palis, J. (2007). The megakaryocyte lineage originates from hemangioblast precursors and is an integral component both of primitive and of definitive hematopoiesis. Blood *109*, 1433–1441.

Wang, Y., Yates, F., Naveiras, O., Ernst, P., and Daley, G.Q. (2005). Embryonic stem cell-derived hematopoietic stem cells. Proc. Natl. Acad. Sci. U S A *102*, 19081–19086.

Willey, S., Ayuso-Sacido, A., Zhang, H., Fraser, S.T., Sahr, K.E., Adlam, M.J., Kyba, M., Daley, G.Q., Keller, G., and Baron, M.H. (2006). Acceleration of mesoderm development and expansion of hematopoietic progenitors in differentiating ES cells by the mouse Mix-like homeodomain transcription factor. Blood *107*, 3122–3130.

Yang, F.C., Atkinson, S.J., Gu, Y., Borneo, J.B., Roberts, A.W., Zheng, Y., Pennington, J., and Williams, D.A. (2001). Rac and Cdc42 GTPases control hematopoietic stem cell shape, adhesion, migration, and mobilization. Proc. Natl. Acad. Sci. U S A *98*, 5614–5618.

Yang, W., and Ernst, P. (2017). Distinct functions of histone H3, lysine 4 methyltransferases in normal and malignant hematopoiesis. Curr. Opin. Hematol. *24*, 322–328.

Yokomizo, T., and Dzierzak, E. (2010). Three-dimensional cartography of hematopoietic clusters in the vasculature of whole mouse embryos. Development *137*, 3651–3661.

Yokomizo, T., Yamada-Inagawa, T., Yzaguirre, A.D., Chen, M.J., Speck, N.A., and Dzierzak, E. (2012). Whole-mount three-dimensional imaging of internally localized immunostained cells within mouse embryos. Nat. Protoc. *7*, 421–431.

Zeisig, B.B., Milne, T., Garcia-Cuellar, M.P., Schreiner, S., Martin, M.E., Fuchs, U., Borkhardt, A., Chanda, S.K., Walker, J., Soden, R., et al. (2004). Hoxa9 and Meis1 are key targets for MLL-ENL-mediated cellular immortalization. Mol. Cell. Biol. *24*, 617–628.

Stem Cell Reports, Volume *14*

Supplemental Information

Enhancing Hematopoiesis from Murine Embryonic Stem Cells through MLL1-Induced Activation of a Rac/Rho/Integrin Signaling Axis

Weiwei Yang, G. Devon Trahan, Elizabeth D. Howell, Nancy A. Speck, Kenneth L. Jones, Austin E. Gillen, Kent Riemondy, Jay Hesselberth, David Bryder, and Patricia Ernst

S1. Establishment and validation of hMLL1 inducible ES cell lines (related to Figure 1)

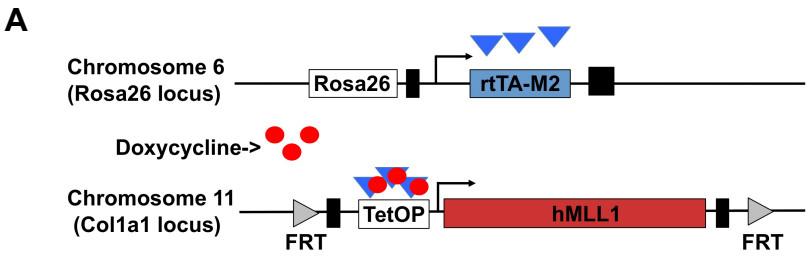

B

Rounds of Screening	Clone Number
Hygromycin Selection	69
Morphology Screen	52
PCR Screen	4
Total Efficiency	5.80%

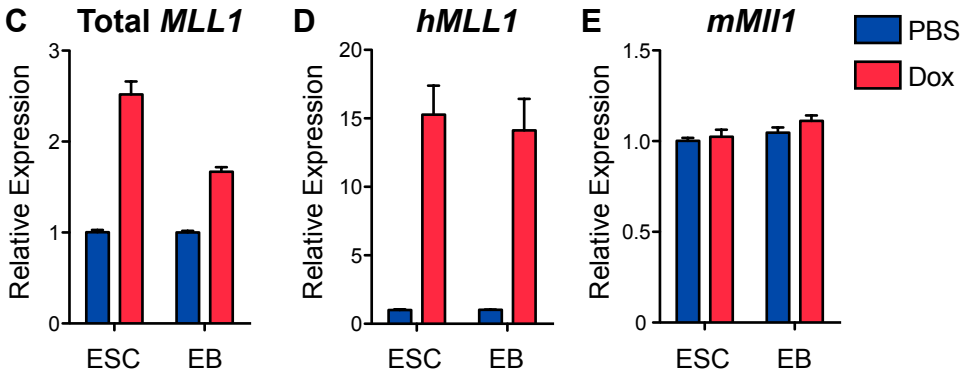

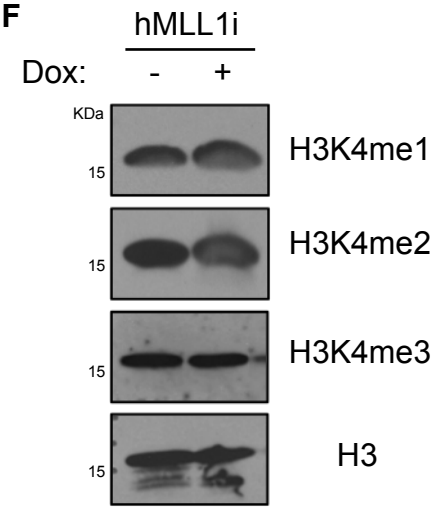

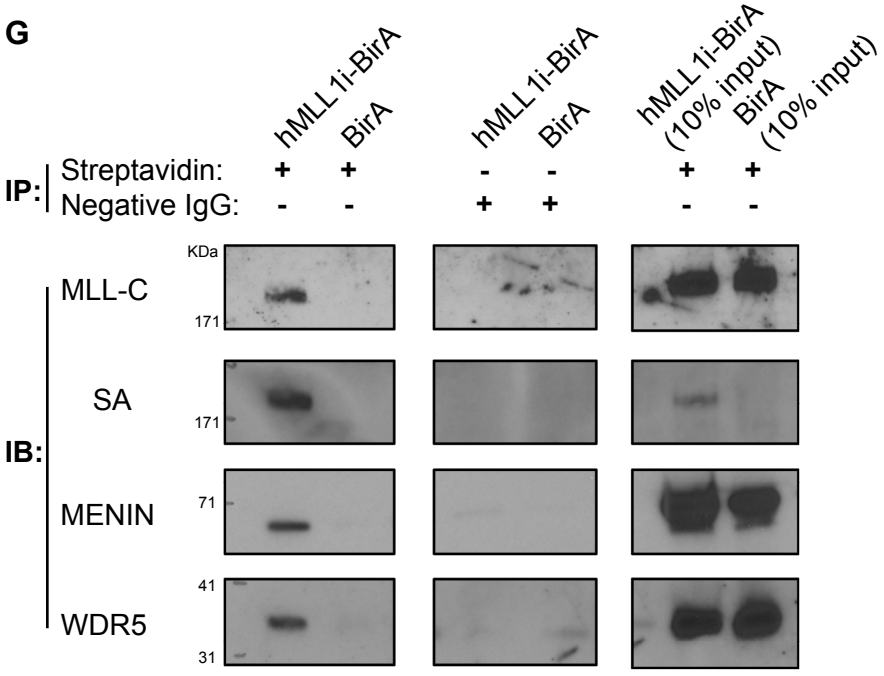

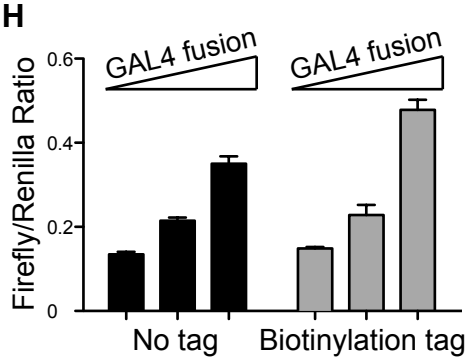

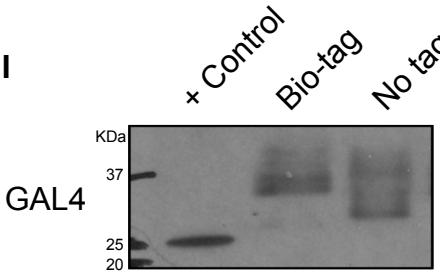

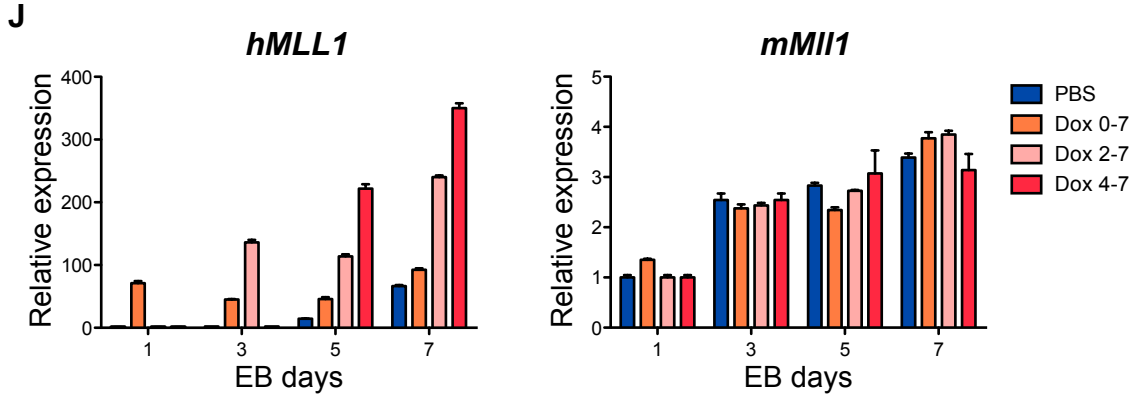

S2. Endothelial and hematopoietic specification is not affected by hMLL1 induction (related to Figure 2)

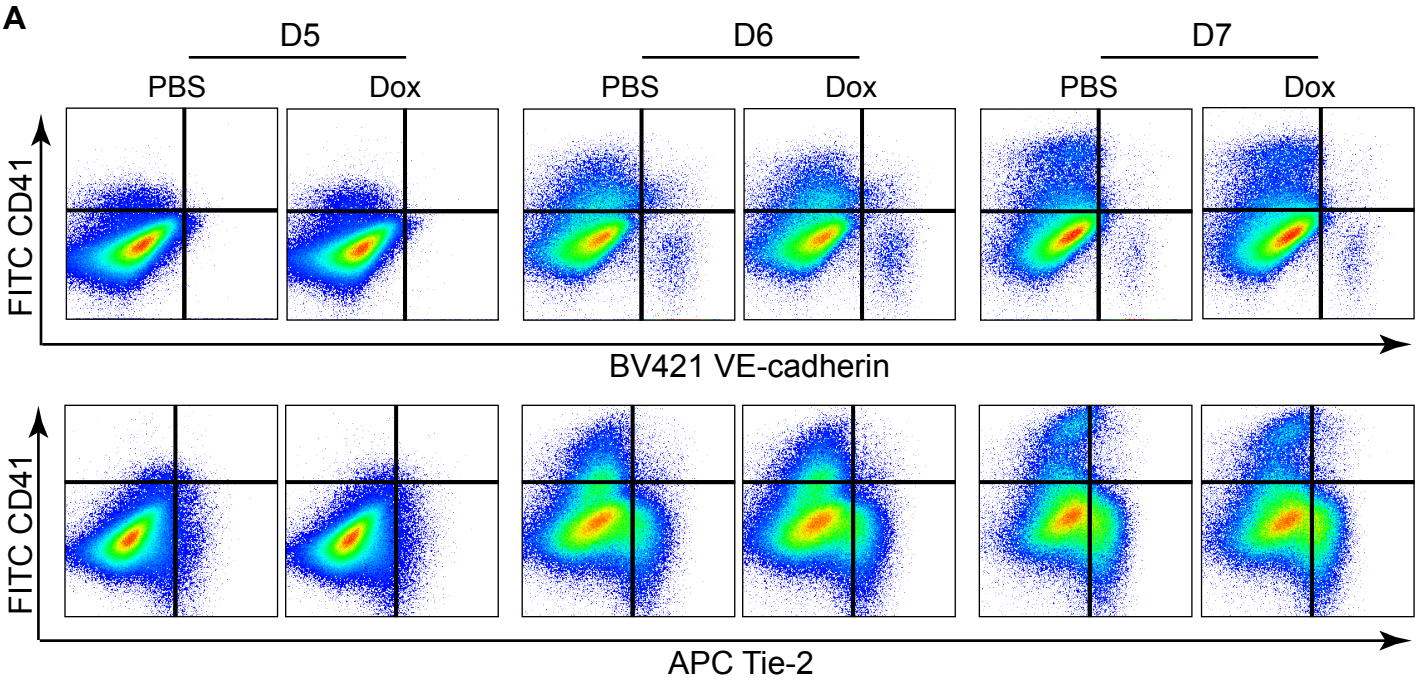

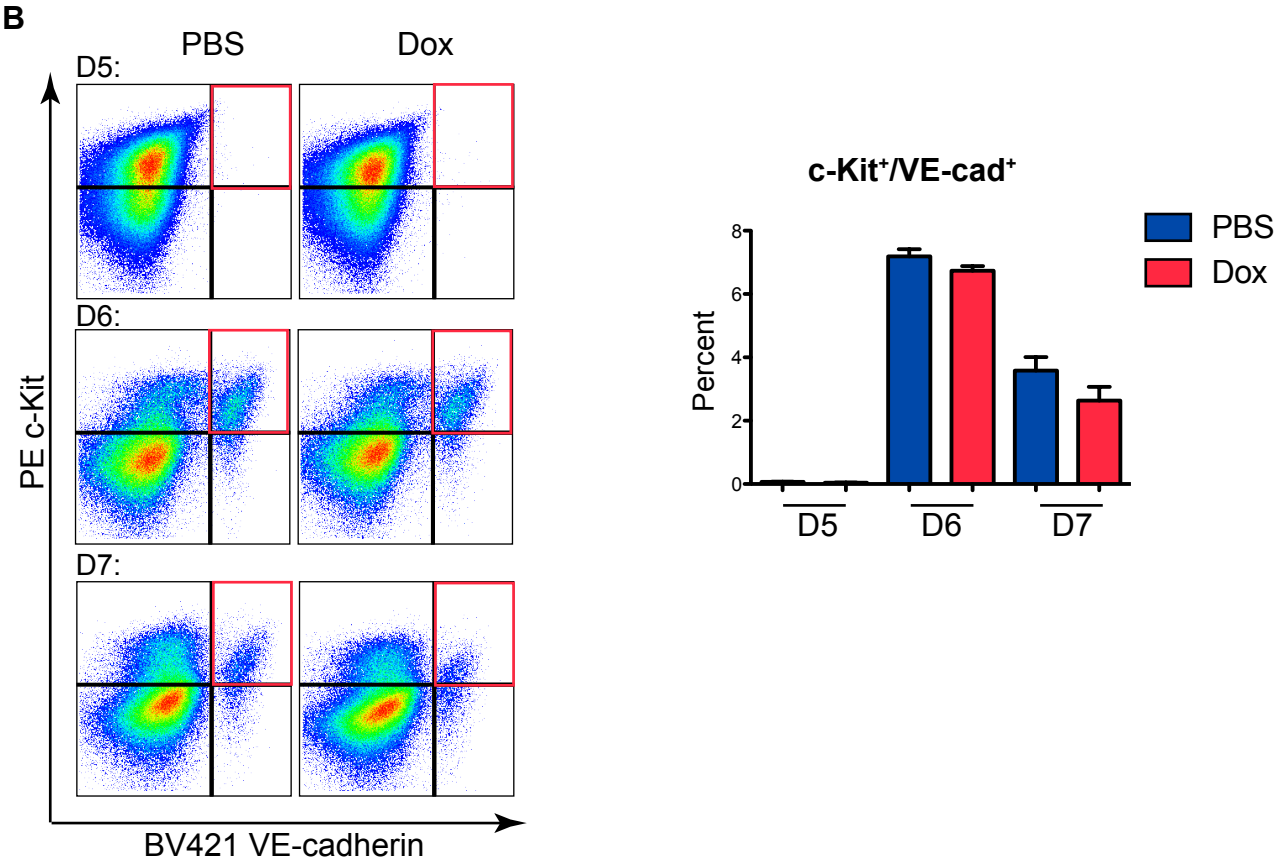

S3. MLL1 increase enhances hematopoietic progenitor activity (related to Figure 3)

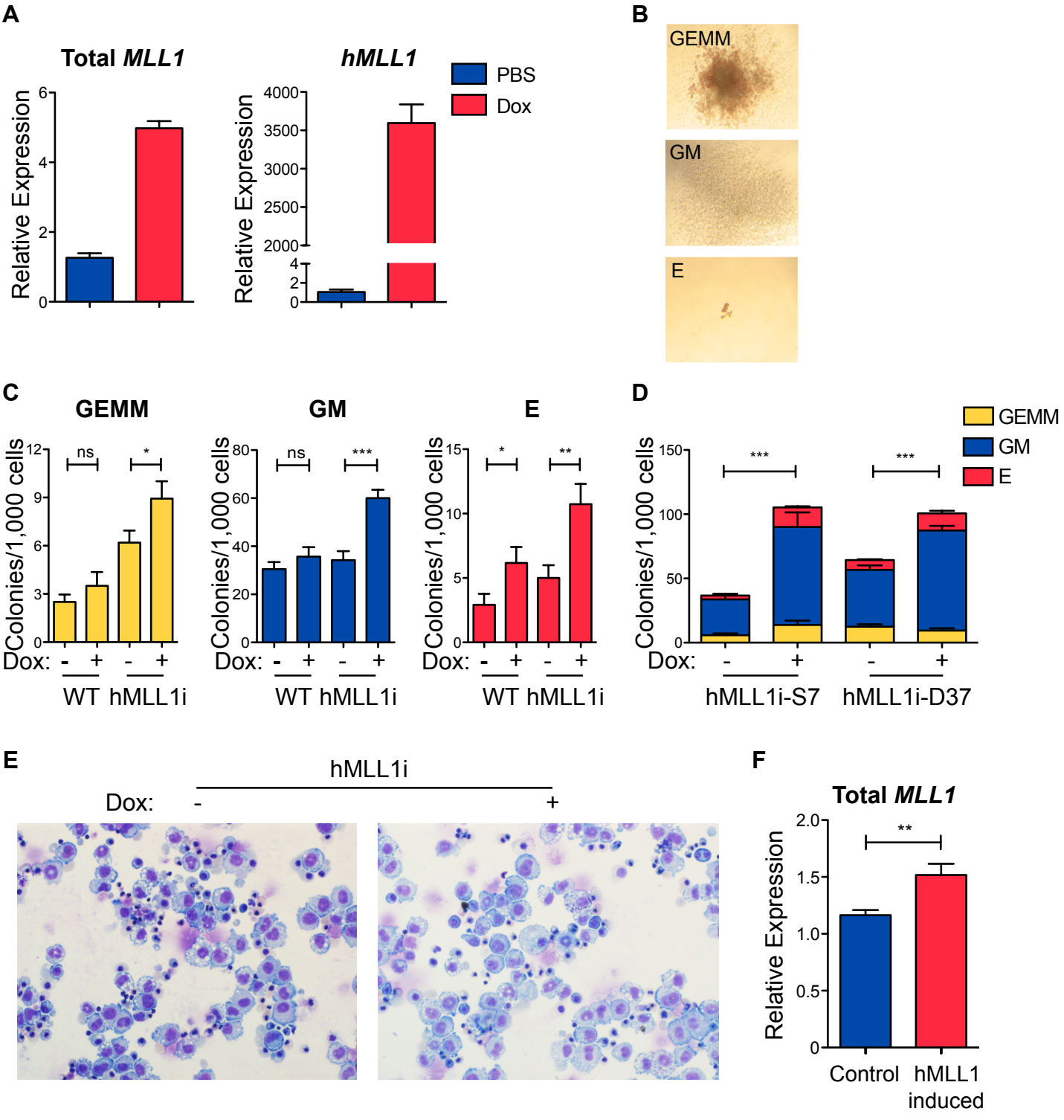

S4. Identification of three clusters from single cell-seq analysis (related to Figure 4)

A

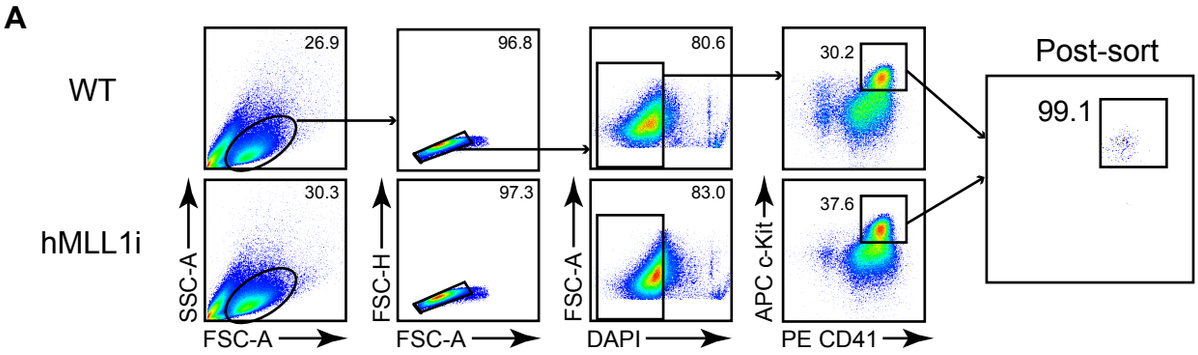

B

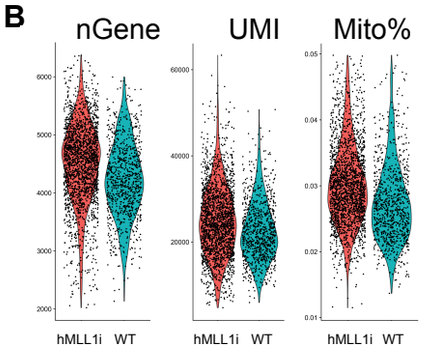

C

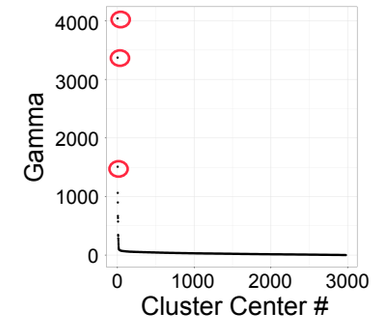

D

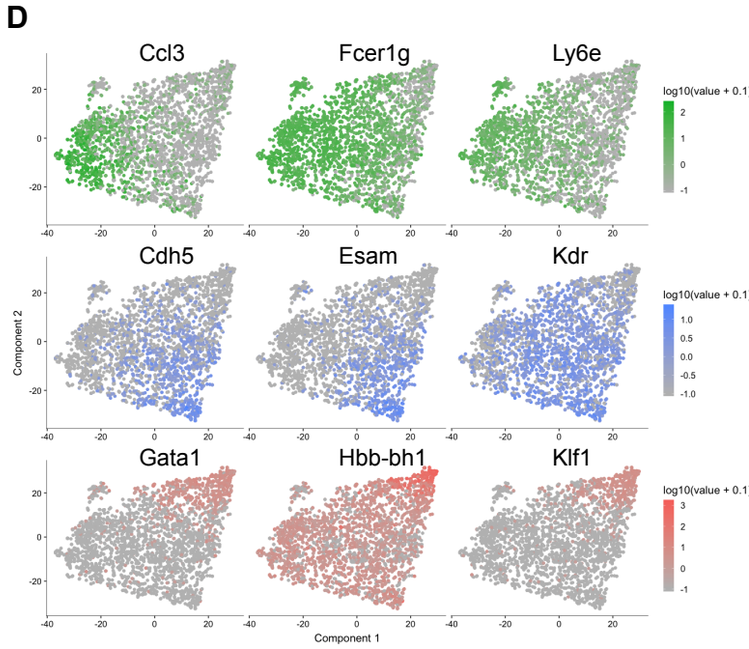

E

GO Terms	p-value
Cluster 1	
Immune system process	4.90E-13
Defense response	5.02E-12
Leukocyte activation involved in immune response	2.02E-10
Myeloid leukocyte differentiation	1.05E-08
Regulation of myeloid cell differentiation	2.61E-08
Cluster 2	
Erythrocyte differentiation	5.83E-05
Regulation of definitive erythrocyte differentiation	7.32E-05
Erythrocyte homeostasis	8.98E-05
Cluster 3	
Regulation of angiogenesis	1.61E-09
Vasculature development	3.70E-09
Regulation of vasculature development	4.40E-09
Positive regulation of angiogenesis	8.53E-09

F

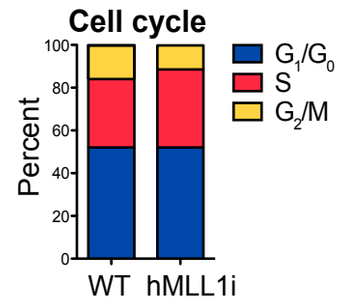

G

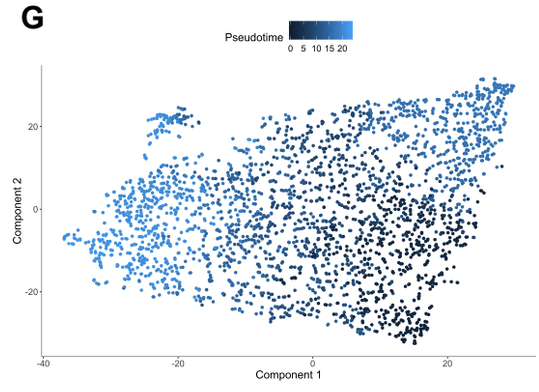

S5. hMLL1 induction activates a Rac/Rho/integrin signaling axis (related to Figure 5)

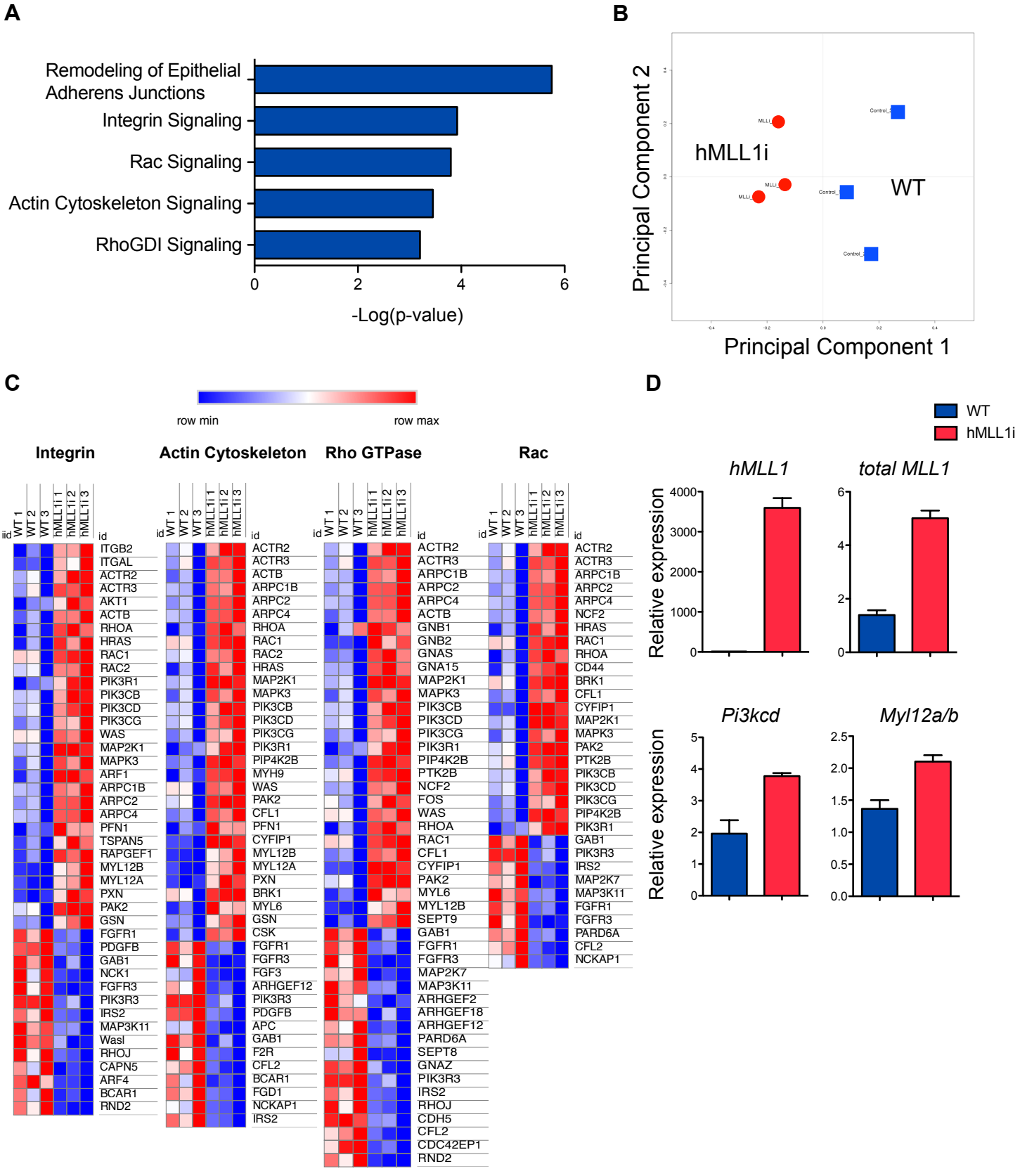

S6. Selective effect of hMLL1 induction on integrins and their activities (related to Figure 6)

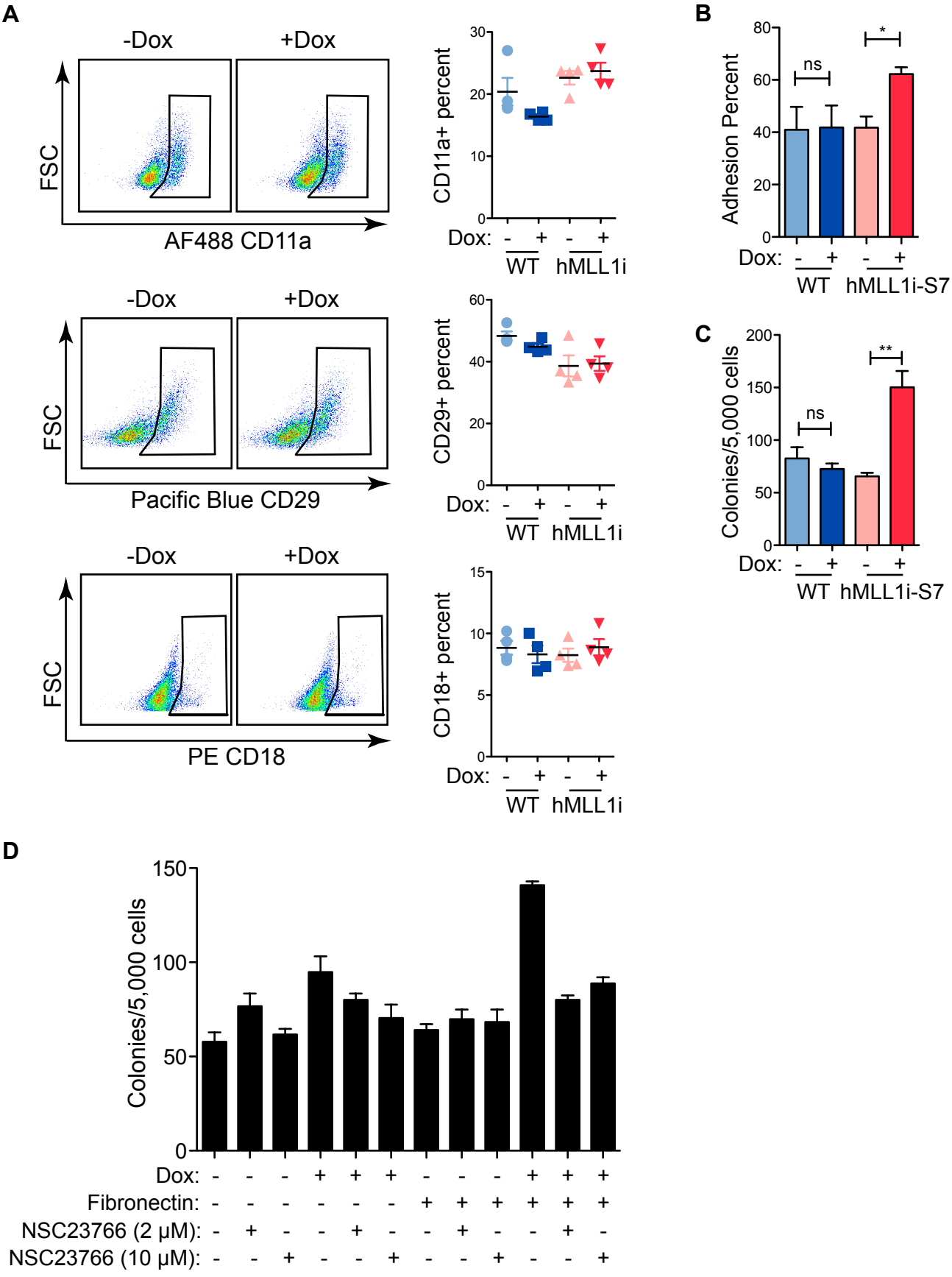

Supplemental Figures:

Figure S1. Establishment and validation of hMLL1 inducible ES cell lines. Related to Figure 1. A) Schematic representation of the MLL1-inducible model. The human MLL1 (hMLL1) cDNA was integrated into the 3' UTR of the *Col1a1* locus under the control of a tetracycline operator (TetOP). Expression of the M2 reverse tetracycline transactivator (rtTA-M2) is driven by the *Rosa26* endogenous regulatory element. **B)** Screening strategy and numbers of clones obtained at each step. Hygromycin selection was performed at 200 µg/mL. The second round of screening selected visually against clones that exhibited differentiated morphology and the final round of screening was determined by PCR with the primers listed in Supplemental Experimental Procedures. Total efficiency refers to correctly targeted clones within the hygromycin-selected pool. **C-E)** Relative induction levels of *hMLL1* transcripts only, total *MLL1* transcripts (including both induced *hMLL1* and endogenous *mMLL1*) and mouse endogenous *Mll1* transcripts in ES and EB (day 6) samples. Data represent average expression (relative to *Gapdh*) +/- SEM, n=3 independent samples each. **F)** H3K4 methylation levels in ES cells. Cells were treated with doxycycline for 48 hrs before histone extraction. Total H3 was used as loading control. **G)** Biotin-tagged hMLL1 interacts with complex components including Menin and Wdr5. Nuclear extracts from BirA ligase stably transfected hMLL1i or control 293 lines were subjected to co-immunoprecipitation with streptavidin or IgG, followed by western blotting with antibodies against the MLL1 c-terminus, Menin and Wdr5. **H)** The presence of an internal biotinylation epitope does not disrupt transactivation by MLL1. Due to the introduction of an epitope tag near the transcriptional activation domain, we tested whether this tagged protein was still capable of transcriptional activation. Gal4-hMLL1 fusion fragments with or without the biotinylation tag were co-transfected with a luciferase reporter and a Renilla internal control plasmid into 293 cells. Luciferase measurements were performed 48 hrs after transfection. One representatve of two experiments is shown. Average normalized relative light units is shown +/- SEM . **I)** Western blotting showing Gal4-hMLL1 proteins. Nuclear extracts were prepared from transiently transfected cells. Bio-tag= Biotin tag. **J**) Relative induction levels of *hMLL1* and mouse *Mll1* in differentiating hMLL1-inducible EBs. Data represent average relative expression (relative to *Gapdh*) +/- SEM, n=3 biological replicates. Legend indicates duration of exposure to doxycycline or PBS control.

Figure S2. Endothelial and hematopoietic specification is not affected by hMLL1 induction. Related to Figure 2. A) Flow cytometry analysis of endothelial and hematopoietic markers c-Kit, VE-cadherin, Tie-2 and Cd41 on EBs at different days of EB differentiation. Experiments were performed using hMLL1 inducible cells. Doxycycline was supplied from day 4 to day 7. **B)** Development of hematopoietic cells from c-Kit+/VE-cadherin+ hemogenic endothelium. Experiments were performed using hMLL1 inducible cells. Dox was supplied from day 4 to day 7. Data is representative of three independent experiments and show averages +/- SEM.

Figure S3. MLL1 increase enhances hematopoietic progenitor activity. Related to Figure 3. A) qRT-PCR shows transcript levels of *hMLL1* and total *MLL1* in the sorted c-Kit+/Cd41+ population. Note that *hMLL1* and total *MLL1* transcript levels are higher in c-Kit+/Cd41+ hematopoietic progenitors than in crude ES/EBs. Data represents average expression (relative to *Gapdh*) +/- SEM, n=3 independent experiments. **B)** Representative colony morphologies from day 7 of the CFU assay. **C**) Colony numbers separated by hematopoietic colony type. GEMM = granulocyte-erythrocyte-monocyte-megakaryocyte; GM = granulocyte-macrophage; E = erythroid. **D)** The increase in hematopoietic potential is a consistent feature of hMLL1 induction. CFU assays were performed on sorted c-Kit+/Cd41+ cells from two additional hMLL1 inducible clones: S7 and D37. One thousand c-Kit+/Cd41+ EB cells were seeded per dish and quantified as in Figure 3. Experiments were performed twice with triplicate dishes each time using clone S7 and once with clone D37; bars show average colonies +/- SEM. **E)** Wright-Giemsa stain of cytospun cells from hMLL1-induced and control CFU plates after 7 days. **F**) Total *(hMLL1 + Mll1)* transcript induction in E9.5 yolk sac cells. Control embryo genotype = rtTA/+ and *hMLL1*/+ animals, n=6; *hMLL1* induced embryo genotype = hMLL1/+; rtTA/+, n=5.

Figure S4. Identification of three clusters from single cell-seq data. Related to Figure 4. A) Cd41+ enriched populations, gating strategy and post-sort analysis is shown for single cell sequencing experiments. **B)** Violin plots showing numbers of gene detected, unique molecular identifiers (UMI) and mitochondrial

gene read percentages post-filtering. **C)** Gamma plot of potential cluster centers from the corresponding t-SNE plot. Data suggests three major clusters circled in red using a gamma threshold of 1500 correpsonding to the three clusters shown in Figure 4. **D)** Marker gene expression for myeloid/innate immune (green), erythroid (red), and HE-like (blue) cells projected onto t-SNE reduced space. Color bars, log10 values of scaled UMI counts. **E)** Gene ontology terms obtained from PANTHER software and p-value of enrichment in the indicated cluster. **F)** Cell cycle analysis derived from analysis of cell cycle related genes (described in Supplemental Experimental Procedures) expressed in single cells. **G)** Developmental progression of cells, as defined by pseudotime, projected onto t-SNE reduced space. Cells are colored corresponding to the three clusters shown in Figure 4.

Figure S5. hMLL1 induction activates a Rac/Rho/integrin signaling axis. Related to Figure 5. A) IPA enrichment of top canonical pathways in cluster 3 "HE-like" population upon hMLL1 induction ordered by *p*-value. **B)** Principal component analysis shows the distribution of individual samples. **C)** Heatmaps of individual gene expression data driving IPA canonical pathways enriched in hMLL1-induced cells. **D)** Validation of gene expression by qRT-PCR using independently sorted samples. Data represents average expression (relative to *Gapdh*) +/- SEM from three independent experiments distinct from the samples used for RNA sequencing.

Figure S6. Selective effect of hMLL1 induction on integrins and their activities. Related to Figure 6. A) Determination of integrin cell surface expression by flow cytometry. Day 6 EB cells were dissociated and stained with antibodies detecting Cd11a (encoded by *Itgal*), Cd18 (encoded by *Itgb2*) and Cd29 (encoded by *Itgb1*). Quantification is shown below as average percentages +/- SEM, n= 4 biological replicates. Data shows one representative experiment of two. **B)** Increased adhesion upon hMLL1 induction reproduced with an additional hMLL1 inducible ES clone, S7. One representative experiment from two is shown as average percentage adherent cells after 24 hrs +/- SEM, n=3 biological replicates. **C)** Increased CFU frequency after fibronectin adhesion reproduced with an independent hMLL1i ES clone, S7. Methods were as described in Figure 6. Bar graph shows one representative experiment of two. Data represents average CFU +/- SEM, n = triplicate cultures. **D)** Primary CFU data and additional doses of Rac1 inhibitor (NSC23766). Data show colonies per 5,000 cells from one representative experiment of two. Shown are average colony numbers +/- SEM, n = triplicate cultures.

Table S1 Differentially expressed genes defining the 3 clusters identified from single cell sequencing data. Related to Figure 4 and Figure S4. Each of three tabs of the excel sheet show the complete list of differentially expressed genes varying by cluster for combined WT and hMLL1i samples. Differentially expressed genes for each cluster were determined using the Seurat FindConservedMarkers function (outlined in Supplemental Experimental Procedures). Normalized gene expression within cells from a particular cluster was compared to expression within cells from all other clusters. Genes with an absolute log fold change less than 0.25 or those expressed in less than 10 percent of cells in either population being compared were excluded from analysis. The pct.1 column represents the fraction of cells expressing at least one transcript of a gene in the cluster in question and pct.2 column represents the fraction of cells expressing that gene in all other clusters.

Supplemental Experimental Procedures:

Generation of hMLL1 inducible ES cell line. A human MLL1 cDNA (hMLL1) from the flag-tagged plasmid spFM11 (Jude et al., 2007) was first modified by introducing a 23 amino acid biotinylation tag (Beckett et al., 1999) within a Xho-SpeI fragment. This fragment was inserted into the full-length human cDNA which was then introduced into the tetracycline-inducible FRT site flanked vector pBS31 (Ugale et al., 2014). The resulting plasmid (pBS-hMLL1-s-bio) was electroporated into KH2 ES cells (Beard et al., 2006) together with the Flp-recombinase plasmid pOG44 to integrate the hMLL1 cDNA into the modified *Col1a1* locus (Figure S1A). Cells were subjected to hygromycin selection for 2 weeks. Correctly integrated clones were identified by screening genomic DNA (Figure S1B) with primers indicated below. The KH2 ES cells were a kind gift of Dr. David Bryder.

Embryos. To generate hMLL1 inducible adults and embryos, ES cells were injected into C57BL/6 blastocysts and chimeric mice identified (Mouse Genetics Core Facility, NJH, Denver), crossed to C57BL/6 mice (The Jackson Laboratory) and speed-backcrossed to generate congenic mice that are at least 95% C57BL/6 by genomic SNP assays before use. Mice were maintained in the animal facilities at University of Colorado, Anschutz Medical Campus. All animal studies were conducted in accordance with IACUC-approved animal protocols at University of Colorado, Anschutz Medical Campus and performed in accord with ethics regulations. Embryos were generated by timed matings between hMLL1;rtTA or C57BL/6 males and females. The day of vaginal plugging (checked at 8 am) was considered embryonic day (E) 0.5 and pregnant females were switched to doxycycline containing (625 mg/kg, Teklad) diet at the day of mating to induce hMLL1 in embryos.

Colony forming unit (CFU) assay. Sorted or Cd41+ enriched cells were seeded respectively at 1,000 or 5,000 cells per mL using M3434 semi-solid medium (StemCell Technologies) containing 1-2 µg/mL doxycycline (Dox). Colonies were scored and/or replated after 7 days culture at 37°C in a 5% CO_2 humidified incubator.

BrdU cell cycle analysis. Proliferation and cell cycle distribution analysis was performed using a bromodeoxyuridine (BrdU) Flow Kit. Sorted day 6 EB cells were culture in liquid medium for 2 days before a 30-minute incubation with BrdU was performed. Cells were then fixed, permeabilized and stained with APC anti-BrdU antibodies and 7-AAD according to the manufacturer's protocol (BD Biosciences).

Western blot. ES cells +/- Dox were harvested and subjected to nuclear/cytoplasmic fractionation using the Dignam procedure. Fifty µg of nuclear extract from each sample was resolved on 3-8% Tris-Acetate Nupage gels (Invitrogen), transferred to nitrocellulose and probed with C-terminal MLL1 rabbit polyclonal antibodies (Hsieh et al., 2003), anti-rabbit HRP conjugate, incubated with ECL reagent (Pierce) and exposed to x-ray film. For histone westerns, nuclear pellets were extracted with 0.25M HCl overnight at 4°C. Ten µg protein was resolved on 15% acrylamide gels, transferred to nitrocellulose and probed with anti-H3K4 mono, di and tri-methylation-specific antibodies (Cell Signaling and Abcam).

Generation of MLL1 293 Flp-in cell line. The full-length *hMLL1* fragment from spFM11 was cloned into pcDNA5/FRT vector (Invitrogen) and cotransfected with pOG44 (Invitrogen) plasmid into the 293 Flp-in cell line (Invitrogen). Stable transfectants were isolated using hygromycin B at 200 µg/mL. Single clones were isolated and expanded. Correctly integrated clones were identified by PCR and lack of beta-galactosidase activity.

Co-immunoprecipitation. Nuclear extract was prepared from BirA-transfected hMLL1i or control 293 cell lines using the Dignam procedure. Two-hundred µg of nuclear extracts were combined with 20 µL pre-washed M280 streptavidin Dynabeads (Invitrogen) and incubated at 4ºC overnight. For a pull-down specificity control, same amount of lysate was incubated with 3 µg mouse IgG and combined with anti-mouse IgG Dynalbeads (Invitrogen) overnight at 4ºC on a rotating stand. Lysate-bead conjugates were washed three times in lysis buffer, eluted in NuPAGE LDS sample buffer (Invitrogen) and resolved by SDS-PAGE using 3-8% Tris-Acetate Nupage gels (Invitrogen). Co-precipitated protein was determined by western blot probed with antibodies as indicated below.

Transactivation assay. Gal4(1-147)-hMLL1 fusion fragments with or without the biotinylation tag were co-transfected with a luciferase reporter (TATA+Inr, (Zenzie-Gregory et al., 1992)) and a Renilla internal control plasmid into 293 cells. Cells were harvested and lysate was used to perform Dual-Luciferase reporter assays (Promega) according to the manufacturer's instructions. Emission from luciferase molecules was measured using Glomax multi detection system (Promega).

Adhesion assay. Plates were coated with 25 µg/mL fibronectin fragment (RetroNectin, Takara) or 10 µg/mL Vcam1 (R&D Systems) overnight at 4°C. Coated plates were blocked with 2% bovine serum albumin for 1 hour and washed three times with phosphate-buffered saline buffer before applying cells for a 30 minute incubation at 37° C, after which non-adherent viable cells were counted using a hemacytometer. The adherent fraction of cells was removed with enzyme-free Cell Dissociation Buffer (Gibco) and counted as above to determine their percentage in the total population. Cells pooled from both adherent and

suspension fractions were seeded into M3434 medium in 35 mm dishes to determine CFU.

Microscopy for EBs and immunofluorescence. Embryoid bodies were photographed using a Cannon Powershot S3 camera mounted to an Olympus CX41 microscope at 40-100x magnifications with a 1951 USAF resolution target to produce accurate scale bars. Enriched Cd41+ cells were subjected to a 24-hour liquid culture on fibronectin coated slides (Neuvitro Corporation). Cells were then fixed with Cytofix/Cytoperm buffer (BD Biosciences) and stained with rhodamine-conjugated phalloidin at 5 U/mL and Hoescht33342 (both from Invitrogen) for DNA content. Images were captured on an Olympus IX83 automated fluorescence microscope. Four representative images containing at least 20 cells per field were used for quantification of cell area using ImageJ software.

Whole-mount immunostaining. E10.5 embryos were fixed in 2% paraformaldehyde/PBS for 20 minutes on ice and then dehydrated in graded concentrations of methanol/PBS (50%, 100%) for 10 minutes each. Embryo trimming and immunostaining for confocal imaging was performed as described (Yokomizo and Dzierzak, 2010). The following primary antibodies were used: rat anti-mouse Cd117 (eBioscience, AB_467434, 1:250), rat anti-mouse Cd31 (BD Pharmingen, AB_396660, 1:500) and rabbit anti-human/mouse Runx1 (Abcam, AB_2049267, 1:250). Secondary antibodies were goat anti-rat Alexa Fluor 647 (Abcam, AB_141778, 1:500), goat-anti rat Alexa Fluor 555 (Invitrogen, AB_141733, 1:1000) and goat anti-rabbit Alexa Fluor 488 (Life Technologies, AB_2576217, 1:1000). Images were acquired on a Zeiss LSM 710 AxioObserver inverted microscope with ZEN 2011 software. The Zeiss LSM 710 is equipped with 488, 543 and 633 nm wavelengths. Images were processed with Fiji software (Schindelin et al., 2012).

Single cell sequencing RNA (scRNAseq), RNA sequencing (RNAseq) and bioinformatics. Day 6 embryoid bodies were dissociated as described above, Cd41+ cells were magnetically enriched, then incubated with c-Kit and Cd41 antibodies (Biolegend). Single cell suspensions were re-suspended in sorting buffer (Hank's Balanced Salt Solution buffer [HBSS] containing 2% FBS) containing 1 µg/mL diamidino-2-phenylindole (DAPI). Singlet-gated, DAPI-negative, c-Kit+/Cd41+ cells were sorted using a FACSAria Fusion. Cell purity was determined by post-sort re-analysis and was typically >90% (Figure S4A). Approximately 4,000-sorted cells were used to generate libraries and sequenced by the University of Colorado Cancer Center Genomics and Microarray core facility. Fastq files for each sample were processed using Cell Ranger 2.0.2. (10x Genomics) with mm10 as the reference genome. The resulting data was then aggregated and normalized using the Cell Ranger aggr pipeline. A total of 4,257 cells (hMLLi, n=2549; parent KH2 control, n=1708) remained following aggregation, with an average of 185,462 reads per cell and a median of 4,091 genes per cell (see Figure S4 for additional quality control).

Expression data for hMLLi and KH2 cells (n = 4,257) was imported into an R environment; the data was filtered and analyzed using the R packages Seurat (Butler et al., 2018) and Monocle (Qiu et al., 2017). Filtering based on unique gene counts less than 2,000, unique molecular identifier (UMI) counts greater than 80,000, or mitochondrial percentages < 1% or > 5% resulted in 2,977 cells in the final analysis, with a average of 24,207 UMI counts per cell and a median of 4,465 genes per cell (Figure S4B). To determine the identities of the clusters, we found it useful to regress out proliferation markers using the algorithm used by the Seurat::Cell Cycle Scoring function (Tirosh et al., 2016). Principal Component Analysis (PCA) was then performed and the top 16 principal components were selected for subsequent use on the basis that each explained at least 1% of the variance observed. The dimensionality was reduced to two dimensions using t-stochastic neighbor embedding (t-SNE)(Maaten and Hinton, 2008), with the 16 principal components being used as input. Cell clusters were demarcated via fast search and find of density peaks (Rodriguez and Laio, 2014) using a gamma threshold of 1,500. Differentially expressed genes were identified for each cluster using the two-sided Student's *t*-test provided by the Seurat FindConservedMarkers function. Normalized gene expression within cells from a particular cluster was compared to expression within cells from all other clusters. Genes with an absolute log fold change less than 0.25 or those expressed in less than 10 percent of cells in either population being compared were excluded from analysis. Following cluster designation, a likelihood ratio test using a generalized linear model was performed to identify genes that vary by cluster. Genes with an adjusted *p*-value of 0.05, an average greater than the bottom quintile of averages, and a dispersion higher than what would be expected using the DESeq model(Anders and Huber, 2010) were then selected to construct a developmental trajectory using DDRTree(Qiu et al., 2017).

Bulk RNA sequencing was performed using sorted c-Kit+/Cd41+ pools of cells from KH2 or hMLL1 induced EB cells incubated with doxycycline from day 4 to day 6. Three separate differentiation experiments were performed with KH2 and hMLL1i differentiated in parallel. Illumina HiSeq libraries were prepared and sequenced by the Genomics and Microarray Core Facility at the University of Colorado Anschutz Medical Campus. Sequenced single-end reads were mapped to the mouse genome (mm10) by GSNAP, expression (FPKM) derived by Cufflinks2, and differential expression analyzed with ANOVA in R.

Gene ontology analysis of single cell RNA seq clusters. Differentially expressed genes (p-value < 0.05) in each cluster were ranked by fold change and top 50 genes were selected to perform gene ontology analysis on the PATHER website (http://www.pantherdb.org/) and confirmed with DAVID v6.8. Additional pathway analyses were performed using Ingenuity Pathway Analysis (Qiagen).

Antibodies used in this study

Western

Antigen	*Host species*	*Catalog*	*Company*
MLL1-C	rabbit polyclonal		in house
Nucleolin (C23)	rabbit polyclonal	sc-13057	Santa Cruz
Streptavidin-HRP	N/A	21130	Thermo Fisher
Wdr5	rabbit polyclonal	13105S	Cell Signaling
Menin	rabbit polyclonal	A300-105A	Bethyl
H3K4me1	rabbit polyclonal	ab8895	Abcam
H3K4me2	rabbit polyclonal	9725S	Cell Signaling
H3K4me3	rabbit polyclonal	ab8580	Abcam
pan-H3	rabbit polyclonal	ab1791	Abcam

Immunofluorescence

Antigen	*Conjugate*	*Catalog*	*Company*
Phalloidin	rhodamine	R415	Invitrogen

Flow Cytometry

Fluorochrome-antibody	*Clone*	*Company*
APC anti-mouse c-Kit	2B8	Biolegend
PE anti-mouse Cd41	MWReg30	Biolegend
FITC anti-mouse Cd41	MWReg30	Biolegend
PE anti-mouse Flk-1	Avas12	Biolegend
PE/Cy7 anti-mouse Pdgfra	APA5	Biolegend
PE anti-mouse c-Kit	2B8	Biolegend
APC anti-mouse Tie-2	TEK4	Biolegend
BV421 anti-mouse Cdh5	BV13	Biolegend
BV421 anti-mouse Cd45	30-F11	Biolegend
APC/Cy7 anti-mouse c-Kit	2B8	Biolegend

BV510 anti-mouse Cd41	MWReg30	Biolegend
FITC anti-mouse Cd34	RAM34	BD Pharmingen
PE/Cy7 anti-mouse Cd16/32	93	Biolegend
APC anti-mouse Mac-1	M1/70	Biolegend
PE anti-mouse Gr-1	R86-8C5	eBioscience
BV421 anti-mouse Sca-1	D7	Biolegend
PE anti-mouse Cd18	M18/2	Biolegend
APC anti-mouse Cd49d	R1-2	Biolegend
AF488 anti-mouse Cd11a	I21/7	Biolegend
Pacific Blue anti-mouse Cd29	HMb1-1	Biolegend

Primers used in this study

Genotyping

Col1-F	5'- TCCCTCACTTCTCATCCAGATATT
Col1-R	5'- AGTCTTGGATACTCCGTGACCATA
SApA-R	5'- GGACAGGATAAGTATGACATCATCAA

qRT-PCR

Gene	Forward primer	Reverse primer
hMLL1	CAGCCAGCCTCCAGTATCTC	TTCCCTTGCATAGGAGCAGT
total MLL1	GCATCTTCTGAGCCAGCAA	GAGGACCCCGGATTAAACAT
Brachyury	CCTCCCTTGTTGCCTTAGAGTAGTT	GCAGATTGTCTTTGGCTACTTTGTC
Flk1	CACCTGGCACTCTCCACCTTC	GATTTCATCCCACTACCGAAAG
Sox1	GCGATGCCAACTTTTGTATG	AGAGGGGATTGCGGTATAAA
Pax6	GTTCCCTGTCCTGTGGACTC	ACCGCCCTTGGTTAAAGTCT
Gata6	CTTGCGGGCTCTATATGAAACTCCAT	TAGAAGAAGAGGAAGTAGGAGTCATAGGGACA
Sox17	GGAGGGTCACCACTGCTTTA	AGATGTCTGGAGGTGCTGCT
Itga4	GAATCCAAACCAGACCTGCGA	TGACGTAGCAAATGCCAGTGG
Itgal	CCAGACTTTTGCTACTGGGAC	GCTTGTTCGGCAGTGATAGAG
Itgb2	CAGGAATGCACCAAGTACAAAGT	CCTGGTCCAGTGAAGTTCAGC
Rac1	ATGCAGGCCATCAAGTGTG	TAGGAGAGGGGACGCAATCT
Rac2	TGCAGGCCATCAAGTGTGTGGT	TAGAGCAGGCTGCAGGGGCGCTT
Rhoa	GCAGGTAGAGTTGGCTTTATGG	TTCTTGTTCCCAACCAGGATGA
Akt1	ATGAACGACGTAGCCATTGTG	TTGTAGCCAATAAAGGTGCCAT
Actb	ATGGATGACGATATCGCT	ATGAGGTAGTCTGTCAGG
Arp3	CAGGCTGAAGTTAAGCGAGGAG	CCTCCAAACCAGACTGCATACC
Pik3cd	ACCATCAGTGGCTCTGCGGTTT	GTGGTCTTCTGGGAACTCACCT
Myl12a/b	CACCATCCAGGAGGATTACC	CTTCAGGATGCGTGTGAACT

Supplemental References:

Anders, S., and Huber, W. (2010). Differential expression analysis for sequence count data. Genome biology *11*, R106.

Beard, C., Hochedlinger, K., Plath, K., Wutz, A., and Jaenisch, R. (2006). Efficient method to generate single-copy transgenic mice by site-specific integration in embryonic stem cells. Genesis *44*, 23-28.

Beckett, D., Kovaleva, E., and Schatz, P.J. (1999). A minimal peptide substrate in biotin holoenzyme synthetase-catalyzed biotinylation. Protein science : a publication of the Protein Society *8*, 921-929.

Butler, A., Hoffman, P., Smibert, P., Papalexi, E., and Satija, R. (2018). Integrating single-cell transcriptomic data across different conditions, technologies, and species. Nature biotechnology *36*, 411-420.

Hsieh, J.J., Ernst, P., Erdjument-Bromage, H., Tempst, P., and Korsmeyer, S.J. (2003). Proteolytic cleavage of MLL generates a complex of N- and C-terminal fragments that confers protein stability and subnuclear localization. Molecular and cellular biology *23*, 186-194.

Jude, C.D., Climer, L., Xu, D., Artinger, E., Fisher, J.K., and Ernst, P. (2007). Unique and independent roles for MLL in adult hematopoietic stem cells and progenitors. Cell stem cell *1*, 324-337.

Maaten, L.v.d., and Hinton, G. (2008). Visualizing Data using t-SNE. Journal of Machine Learning Research *9*, 2579-2605.

Qiu, X., Mao, Q., Tang, Y., Wang, L., Chawla, R., Pliner, H.A., and Trapnell, C. (2017). Reversed graph embedding resolves complex single-cell trajectories. Nature methods *14*, 979-982.

Rodriguez, A., and Laio, A. (2014). Machine learning. Clustering by fast search and find of density peaks. Science *344*, 1492-1496.

Schindelin, J., Arganda-Carreras, I., Frise, E., Kaynig, V., Longair, M., Pietzsch, T., Preibisch, S., Rueden, C., Saalfeld, S., Schmid, B.*, et al.* (2012). Fiji: an open-source platform for biological-image analysis. Nature methods *9*, 676-682.

Tirosh, I., Izar, B., Prakadan, S.M., Wadsworth, M.H., 2nd, Treacy, D., Trombetta, J.J., Rotem, A., Rodman, C., Lian, C., Murphy, G.*, et al.* (2016). Dissecting the multicellular ecosystem of metastatic melanoma by single-cell RNA-seq. Science *352*, 189-196.

Ugale, A., Norddahl, G.L., Wahlestedt, M., Sawen, P., Jaako, P., Pronk, C.J., Soneji, S., Cammenga, J., and Bryder, D. (2014). Hematopoietic stem cells are intrinsically protected against MLL-ENL-mediated transformation. Cell reports *9*, 1246-1255.

Yokomizo, T., and Dzierzak, E. (2010). Three-dimensional cartography of hematopoietic clusters in the vasculature of whole mouse embryos. Development *137*, 3651-3661.

Zenzie-Gregory, B., O'Shea-Greenfield, A., and Smale, S.T. (1992). Similar mechanisms for transcription initiation mediated through a TATA box or an initiator element. The Journal of biological chemistry *267*, 2823-2830.